Article

Molecular basis for differential *Igk* versus *Igh* V(D)J joining mechanisms

https://doi.org/10.1038/s41586-024-07477-y

Received: 26 January 2024

Accepted: 26 April 2024

Published online: 29 May 2024

Open access

Check for updates

Yiwen Zhang[1,2,6], Xiang Li[1,2,6], Zhaoqing Ba[1,2,3], Jiangman Lou[1,2,4], K. Elyse Gaertner[1,2,5], Tammie Zhu[1,2], Xin Lin[1,2], Adam Yongxin Ye[1,2], Frederick W. Alt[1,2]✉ & Hongli Hu[1,2,6]✉

In developing B cells, V(D)J recombination assembles exons encoding IgH and Igκ variable regions from hundreds of gene segments clustered across *Igh* and *Igk* loci. V, D and J gene segments are flanked by conserved recombination signal sequences (RSSs) that target RAG endonuclease[1]. RAG orchestrates *Igh* V(D)J recombination upon capturing a J_H-RSS within the J_H-RSS-based recombination centre[1–3] (RC). J_H-RSS orientation programmes RAG to scan upstream D- and V_H-containing chromatin that is presented in a linear manner by cohesin-mediated loop extrusion[4–7]. During *Igh* scanning, RAG robustly utilizes only D-RSSs or V_H-RSSs in convergent (deletional) orientation with J_H-RSSs[4–7]. However, for Vκ-to-Jκ joining, RAG utilizes Vκ-RSSs from deletional- and inversional-oriented clusters[8], inconsistent with linear scanning[2]. Here we characterize the Vκ-to-Jκ joining mechanism. *Igk* undergoes robust primary and secondary rearrangements[9,10], which confounds scanning assays. We therefore engineered cells to undergo only primary Vκ-to-Jκ rearrangements and found that RAG scanning from the primary Jκ-RC terminates just 8 kb upstream within the CTCF-site-based *Sis* element[11]. Whereas *Sis* and the Jκ-RC barely interacted with the Vκ locus, the CTCF-site-based *Cer* element[12] 4 kb upstream of *Sis* interacted with various loop extrusion impediments across the locus. Similar to V_H locus inversion[7], DJ_H inversion abrogated V_H-to-DJ_H joining; yet Vκ locus or Jκ inversion allowed robust Vκ-to-Jκ joining. Together, these experiments implicated loop extrusion in bringing Vκ segments near *Cer* for short-range diffusion-mediated capture by RC-based RAG. To identify key mechanistic elements for diffusional V(D)J recombination in *Igk* versus *Igh*, we assayed Vκ-to-J_H and D-to-Jκ rearrangements in hybrid *Igh*–*Igk* loci generated by targeted chromosomal translocations, and pinpointed remarkably strong Vκ and Jκ RSSs. Indeed, RSS replacements in hybrid or normal *Igk* and *Igh* loci confirmed the ability of *Igk*-RSSs to promote robust diffusional joining compared with *Igh*-RSSs. We propose that *Igk* evolved strong RSSs to mediate diffusional Vκ-to-Jκ joining, whereas *Igh* evolved weaker RSSs requisite for modulating V_H joining by RAG-scanning impediments.

Bona fide RSSs flanking antigen receptor gene segments have a conserved palindromic heptamer with a consensus CACAGTG sequence and a less-conserved AT-rich nonamer separated by 12-bp or 23-bp spacers[1] (denoted 12RSSs and 23RSSs, respectively). RAG endonuclease initiates V(D)J recombination by cleaving between the CAC of the heptamer and flanking coding sequences upon capturing complementary 12RSSs and 23RSSs in its two active sites, a property known as 12/23 restriction[1,13,14]. In the mouse *Igh*, more than 100 V_H segments lie within a 2.4 Mb distal portion followed downstream by multiple D segments and four J_H segments[2]. V_H segments have downstream 23RSSs, D segments have 12RSSs on both sides, and J_H segments have upstream 23RSSs[2]. Owing to 12/23 restriction, V_H segments cannot directly join to J_H segments. In progenitor B (pro-B) cells, joining of all D segments, except proximal DQ52, to J_H segments occurs via linear scanning during which RAG dominantly captures and utilizes downstream, deletional D-12RSSs owing to convergent orientation with J_H-23RSSs[5]. As DQ52 lies within the *Igh*-RC, both of its RSSs access RAG by short-range diffusion, but the downstream DQ52-12RSS predominates owing to its superior strength[2,5,15]. The DJ_H intermediate and its upstream 12RSS form a RC for V_H-to-DJ_H joining[2,3]; but the IGCR1 regulatory region just upstream of the D segments contains two CTCF-binding elements (CBEs) that substantially impede upstream RAG scanning[4,6,16]. Moreover, most D-proximal V_H segments have RSS-associated CBEs that impede RAG scanning and enhance their interaction with the DJ_H-RC, increasing their utilization

[1]Howard Hughes Medical Institute, Program in Cellular and Molecular Medicine, Boston Children's Hospital, Boston, MA, USA. [2]Department of Genetics, Harvard Medical School, Boston, MA, USA. [3]Present address: National Institute of Biological Sciences, Beijing, China. [4]Present address: Copenhagen University, Copenhagen, Denmark. [5]Present address: Georgetown University, Washington, DC, USA. [6]These authors contributed equally: Yiwen Zhang, Xiang Li, Hongli Hu. ✉e-mail: alt@enders.tch.harvard.edu; hongli.hu@childrens.harvard.edu

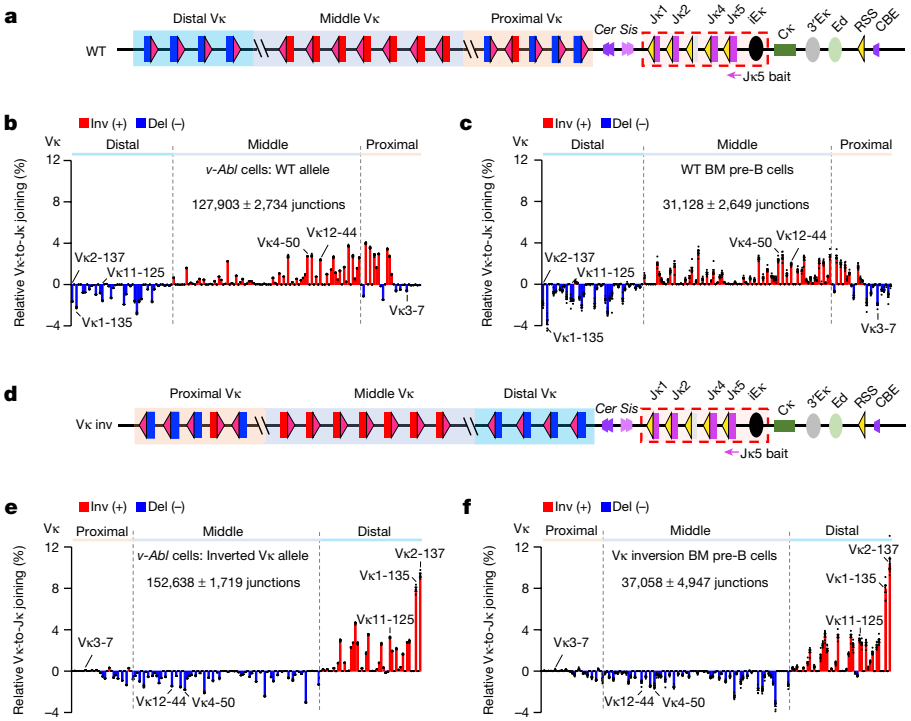

Fig. 1 | Vκ locus inversion maintains utilization of deletional and inversional Vκ segments in bone marrow pre-B cells and in *v-Abl* cells. a, Illustration of mouse *Igk* (not to scale). Relative location of proximal (orange shadow) and distal (blue shadow) mainly deletional-oriented Vκ segments and middle (grey shadow) mainly inversional-oriented Vκ segments. *Cer* and *Sis* lie downstream of the proximal Vκ; *Cer* upstream-oriented (purple trapezoids) and *Sis* downstream-oriented (pink trapezoids) CBEs are indicated. Four functional Jκ segments downstream of *Sis*, with the *Igk* intronic enhancer (iEκ), form the RC (dashed red rectangle). Further downstream, the Cκ, *Igk* enhancers, RSS and upstream-oriented CBE are indicated. Vκ segments are flanked by 12RSSs (red triangles) and Jκ segments by 23RSSs (yellow triangles). Vκ locus CBEs are shown in Fig. 2. WT, wild type. **b**,**c**, Relative utilization of individual Vκ segments on wild-type alleles in *v-Abl* cells (**b**) and bone marrow (BM) pre-B cells (**c**) baiting from Jκ5 (indicated in **a**). Inv, inversional joins; Del, deletional joins. Locations of selected Vκ segments are indicated—these features are retained in subsequent figures. Vκ usage patterns in **b**,**c** are highly similar (two-sided Pearson's $r = 0.88$, $P = 2.2 \times 10^{-53}$). **d**, Illustration of inverted Vκ locus. **e**,**f**, Relative utilization of individual Vκ segments on inverted Vκ alleles in *v-Abl* cells (**e**) and bone marrow pre-B cells (**f**) assayed with Jκ5 bait. Vκ usage data in the inverted locus is shown in the inverted orientation. Vκ usage patterns in **e**,**f** are highly similar (two-sided Pearson's $r = 0.97$, $P = 5.5 \times 10^{-97}$). Junction numbers are shown in each panel and in subsequent figures for comparison of absolute levels. Vκ utilization data are presented as mean ± s.e.m. from 4 (**b**,**e**) or 7 (**c**,**f**) biological repeats.

far beyond that provided by their RSSs alone[3]. To promote balanced V_H utilization, the activity of CBEs and other V_H locus scanning impediments is diminished in pro-B cells by developmental down-modulation of the WAPL cohesin-unloading factor[7,17], enabling linear loop extrusion to directly present the entire V_H locus to the RAG-bound DJ_H-RC[7]. Although RAG linearly scans the length of an inverted V_H locus, V_H-to-DJ_H joining is nearly abrogated due to bona fide V_H-RSSs no longer being in convergent orientation with the DJ_H-RC RSS[7].

Primary Vκ-to-Jκ joining does not use RAG scanning

The distal 3 Mb of mouse *Igk* contains 103 functional Vκ segments associated with 12RSSs followed downstream by the *Igk*-RC that contains 4 functional Jκ segments with 23RSSs, allowing direct Vκ-to-Jκ joining[8] (Fig. 1a). The *Cer* and *Sis* elements, each of which contain two CBEs and are located in the 13 kb interval between the most proximal Vκ and Jκ1 (Fig. 1a), functionally promote distal Vκ usage[11,12]. In precursor B (pre-B) cells, initial (primary) Vκ-to-Jκ rearrangements mostly utilize Jκ1[18]. Subsequently, the three functional downstream Jκ segments (Jκ2, Jκ4 and Jκ5) undergo secondary rearrangements with remaining upstream Vκ segments[18]. V(D)J recombination, which occurs strictly in the G1 phase of the cell cycle[19], can be activated in G1-arrested Abelson murine leukaemia virus-transformed pro-B cell lines[20] (hereafter referred to as '*v-Abl* cells'). For high-throughput genome-wide translocation sequencing-adapted V(D)J-sequencing (HTGTS-V(D)J-seq) assays[21], we generated RAG-deficient *v-Abl* cells and ectopically introduced RAG upon G1 arrest. Although *v-Abl* cells undergo robust D-to-J_H rearrangements, they rarely exhibit V_H-to-DJ_H rearrangements owing to high levels of WAPL[7]. Despite these high WAPL levels, *v-Abl* cells underwent robust Vκ-to-Jκ rearrangements with usage patterns of deletional- and inversional-oriented Vκ segments similar to those of normal bone marrow pre-B cells (Fig. 1b,c). Of note, bone marrow pre-B cells and *v-Abl* cells in which we inverted the Vκ locus (Fig. 1d) underwent very similar patterns of robust Vκ-to-Jκ rearrangements, with previously deletional-oriented Vκ segments rearranging by inversion and previously inversional-oriented Vκ segments rearranging by deletion (Fig. 1e,f). These results confirm that *Igk* utilizes a markedly different long-range V(D)J recombination mechanism to that of *Igh* and indicate that *v-Abl* lines are a faithful system for in depth analyses of this mechanism.

To facilitate the assessment of effects of *cis*-acting *Igk* modifications in *v-Abl* cells, we generated a *v-Abl* cell line containing a single *Igk* locus (the single *Igk* allele *v-Abl* line). This line undergoes Vκ-to-Jκ joining nearly identically to its parental line (Fig. 2a,b; compare with Fig. 1b). Long-range RAG chromatin scanning of both the *Igh* and other multi-megabase domains genome-wide can be revealed by highly sensitive HTGTS-V(D)J-seq-based RAG-scanning assays for very low-level RAG-initiated joins between a RC-based bona fide RSS and weak cryptic RSSs as simple as the CAC of the heptamer when in convergent orientation[2,4,5,7]. This assay reveals chromatin regions scanned by RC-based RAG, directionality of exploration, and effects of local chromatin structure on loop extrusion-mediated scanning activity[2,4,5,7]. We used

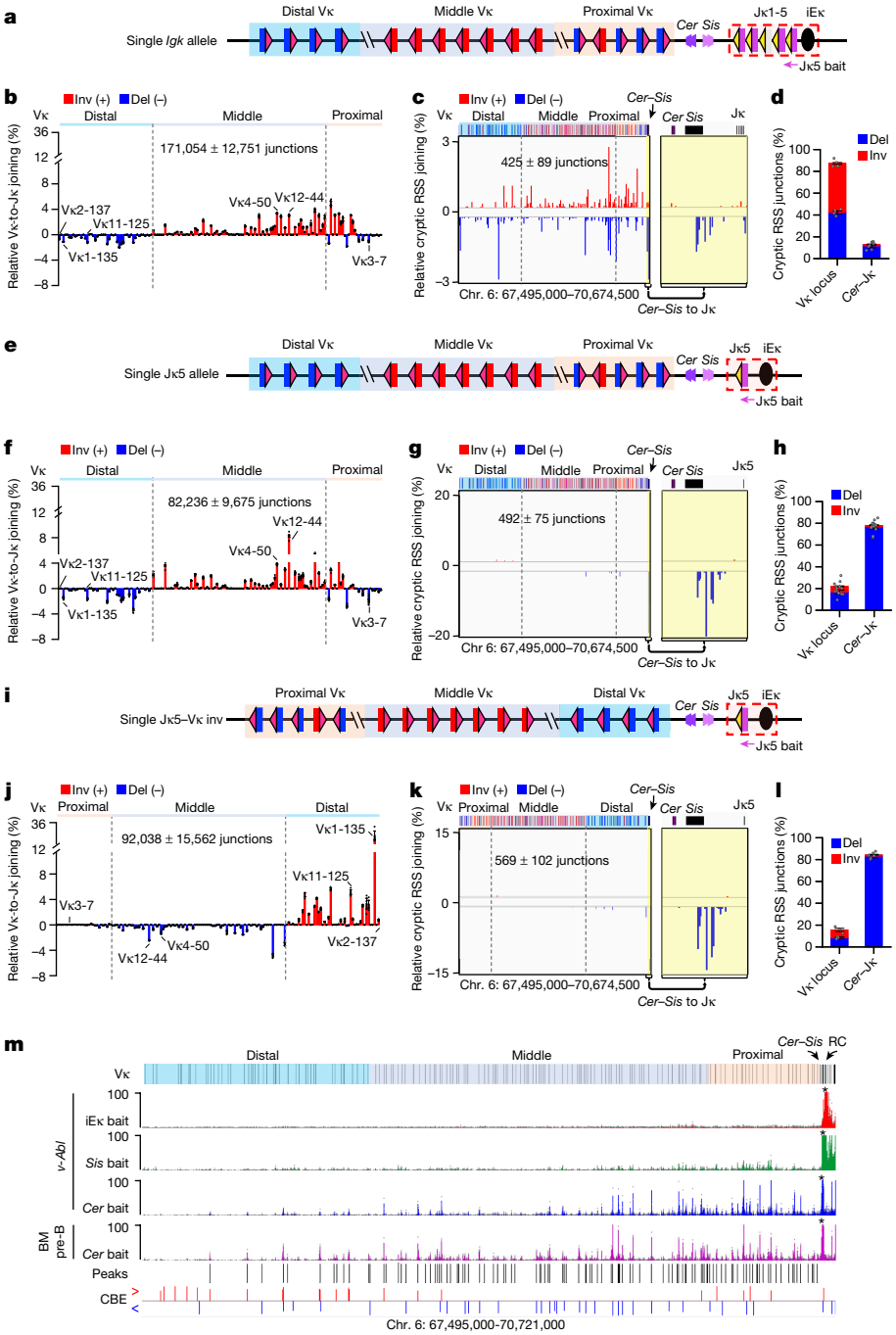

Fig. 2 | RAG scanning for primary *Igk* rearrangement is terminated within *Sis* while *Cer* interacts across the Vκ locus. a, Diagram of the single *Igk* allele *v-Abl* line. **b**, Relative utilization of individual Vκ segments in the single *Igk* allele line with Jκ5 bait. **c**, Percentage of pooled RAG off-target junctions in *Igk* locus from the single *Igk* allele line. The region between *Cer* and Jκ, highlighted in yellow, is enlarged on the right. **d**, Percentage of inversional and deletional cryptic RSS junctions within indicated Vκ locus (chromosome (chr.) 6:67,495,000–70,657,000) and *Cer*–Jκ regions (chr. 6:70,657,000–70,674,500) from the single *Igk* allele line. **e**, Diagram of the single Jκ5 allele *v-Abl* line. **f**–**h**, Vκ usage (**f**) and RAG off-target profiles (**g**,**h**) in the single Jκ5 allele line presented as in **b**–**d**. **i**, Diagram of the single Jκ5-Vκ inv *v-Abl* line. **j**–**l**, Vκ usage (**j**) and RAG off-target profiles (**k**,**l**) in the single Jκ5-Vκ inv line presented as in **b**–**d**. Vκ1-135 is over-utilized (**j**), probably owing to its associated transcription. In Fig. 1e,f, Vκ2-137 is equally used, probably owing to its replacement of primary Vκ1-135 inversional rearrangements via deletional secondary rearrangements. Vκ usage data and RAG off-target junctions in the inverted locus are shown in inverted orientation (**j**,**k**). **m**, Chromosome conformation capture (3C)-HTGTS profiles in the *Igk* locus from RAG-deficient *v-Abl* cells baiting from iEκ (red), *Sis* CBE2 (green) and *Cer* CBE1 (blue) and from RAG-deficient primary pre-B cells baiting from *Cer* CBE1 (pink). Asterisks indicate the location of baits. Locations of *Cer*-baited interaction peaks in the Vκ locus significantly above background are indicated with black lines, CBEs in the *Igk* locus are indicated with red (rightward) and blue (leftward) lines. Details on peak calling are provided in Methods. Vκ utilization and cryptic RSS data are presented as mean ± s.e.m. from 4 (**b**,**d**), 7 (**f**,**h**) or 3 (**j**,**l**) biological repeats; 3C-HTGTS data are presented as mean value from 2 biological repeats.

this assay with a Jκ5 bait, which should primarily detect chromosomal joins[8], to assess RAG scanning versus normal Vκ-to-Jκ joining activity in the single *Igk* allele *v-Abl* line. The results were markedly different from linear strand-specific scanning tracks observed during V_H-to-DJ_H rearrangement[6,7]; indeed, scanning tracks appeared across the Vκ locus on both DNA strands and lacked clear directionality (Fig. 2c,d). These

scanning patterns suggested that inversional rearrangements displace *Cer* and *Sis* impediments and place groups of downstream inversional Vκ segments in deletional-orientation upstream of remaining Jκ segments for secondary rearrangements[9,10], potentially mediated by linear RAG scanning.

To more rigorously test the origin of the complex wild-type *v-Abl Igk* scanning patterns, we deleted both Jκ1-4 and the downstream *Igk*-RSS-based deleting element[22] from the single *Igk* allele *v-Abl* cells, leaving Jκ5 in its normal position relative to iEκ. This 'single Jκ5 allele' *v-Abl* line undergoes only primary Vκ-to-Jκ5 rearrangements (Fig. 2e), with rearrangements and scanning patterns representing those that happen during primary Vκ-to-Jκ recombination. Primary bona fide Jκ5 joins to deletional and inversional Vκ segments across the locus were chromosomally retained with patterns somewhat different from those of the parental single *Igk* allele *v-Abl* cells (Fig. 2f; compare with Fig. 2b), probably owing in large part to elimination of secondary rearrangements (see Fig. 2 caption). However, overall findings were clear—primary RAG scanning from the Jκ5-based RC was terminated 8 kb upstream within *Sis* (Fig. 2g,h), despite primary Vκ-to-Jκ joins in the same cells occurring across the locus (Fig. 2f). We also inverted the Vκ locus in the single Jκ5 allele *v-Abl* line to form the 'single Jκ5–Vκ inv' line (Fig. 2i). In the single Jκ5–Vκ inv *v-Abl* line, Vκ-to-Jκ rearrangements occurred across the locus, albeit with dominant utilization of the normally distal Vκ1-135 in a proximal position (Fig. 2j); however, primary RAG scanning was still terminated within *Sis* (Fig. 2k,l). Finally, we generated a single Jκ1 allele *v-Abl* line and found that Vκ segments were utilized across the locus (Extended Data Fig. 1a,b); but primary RAG scanning was also terminated within *Sis* (Extended Data Fig. 1c,d).

Primary Vκ-to-Jκ joining uses short-range diffusion

Given our findings that RAG does not linearly scan upstream chromatin beyond *Sis* during primary Vκ-to-Jκ rearrangement, we used high-resolution 3C-HTGTS[3] to explore interactions of the *Igk*-RC, *Sis* or *Cer* with the Vκ locus in RAG-deficient *v-Abl* cells. These analyses revealed that, compared with *Cer*, the *Igk*-RC and *Sis* had little interaction with sequences upstream of *Cer* (Fig. 2m, top 3 tracks). By contrast, *Cer* interacted with more than 100 sites across the Vκ locus in RAG-deficient pre-B cells, many of which were also found in RAG-deficient *v-Abl* lines (Fig. 2m, bottom two tracks). Moreover, *Cer* did not interact substantially with *Igk* sequences, including the RC, downstream of *Sis* (Extended Data Fig. 2a). The strongest *Cer* interactions frequently corresponded to CBEs[23], but many others corresponded to E2A sites, often in association with transcribed sequences (Extended Data Fig. 2b and Supplementary Data 1). Notably, two previously described Vκ enhancers were in the latter category; deletion of either enhancer affected utilization of nearby Vκ segments[24,25]. As these deletions were done in wild-type cells, additional effects of the enhancer deletions on primary *Igk* rearrangements might be confounded by secondary rearrangements (see example in Fig. 2 caption). Finally, it is notable that these interactions with the *Cer* bait across the Vκ locus occurred with WAPL levels that abrogate interactions of IGCR1 CBE with upstream V_H locus scanning impediments[6,26,27]. In this regard, CBEs in the Vκ locus appear less dense and less potent than those in the V_H locus (Extended Data Fig. 3a,b). Thus, loop extrusion may proceed more readily across the Vκ locus with high WAPL levels, as found for other multi-megabase loci without strong extrusion impediments in *v-Abl* cells[4]. Internal convergent CBE-based loops in the Vκ locus have been proposed as a major mechanism for bringing Vκ segments into proximity with *Cer*[23]. Our current findings support a mechanism in which juxtaposition of Vκ segments with the *Cer* anchor is mediated by ongoing loop extrusion. During this process CBEs, E2A sites and transcribed sequences act as dynamic impediments[5] to extend the time for short-range diffusional interactions of Vκ segments with the *Igk*-RC. Transcription can further increase accessibility of RSSs to RAG[28].

Igk-specific elements promote diffusional joining

To further explore the basis for the differential V(D)J recombination mechanisms in the *Igh* versus *Igk* loci, we generated pre-rearranged DQ52J_H4 (DJ_H-WT) and inverted DQ52J_H4 (DJ_H-inv) *v-Abl* lines in which WAPL could be depleted (Fig. 3a). In the DJ_H-WT *v-Abl* line, WAPL depletion activated V_H-to-DJ_H joining and RAG scanning across the V_H locus (Fig. 3c,e, top, g, left). In the WAPL-depleted DJ_H-inv *v-Abl* line, V_H-to-DJ_H rearrangement was abrogated and RAG scanning was directed downstream through the *Igh* locus to the 3′ CBE cluster (Fig. 3c,e, bottom, g, right). This finding is notable, as it has been suggested that inverting the V_H locus affects V_H-to DJ_H rearrangement by disrupting convergent V_H locus CBE-based structure[17]. Our findings from the DJ_H inversion rule out this possibility, as the inversion does not alter any CBEs in the *Igh* locus or elsewhere and leaves the RC DJ_H inverted in its normal location. Rather, the DJ_H inversion only affects the direction of RAG chromatin scanning from the RC. For comparison, we also inverted Jκ5 in the single Jκ5 allele line to generate the 'single Jκ5-inv' line (Fig. 3b). Indeed, the Jκ5 inversion redirected RC-bound RAG to scan *Igk* chromatin downstream of the RC to the 3′ *Igk* CBE (Fig. 3f,h). However, other than reversing the orientation by which different Vκ segments joined to the Jκ5, there was little effect on the utilization of upstream Vκ segments across the locus (Fig. 3d). In this regard, as cryptic RSS-based scanning reflects cohesin-mediated loop extrusion past the RC, rather than movement of the RC itself, the inverted Jκ5 would not alter the position of Jκ5-RC-bound RAG relative to *Sis* for short-range diffusional capture of bona fide Vκ-RSSs extruded past *Cer*. These findings from Jκ inversion strongly support the short-range diffusion model for Vκ access to the Jκ-RC and suggest that the *Igk* locus, but not the *Igh* locus, has elements that promote this process.

Hybrid loci reveal *Igk*-specific elements

The next major question was to identify the key elements that enable a diffusion-based RC access mechanism to robustly function in *Igk* and not in *Igh*[2]. To address this question, we performed mix-and-match experiments between portions of the two loci. To facilitate these experiments, we used a CRISPR–Cas9-mediated chromosomal translocation targeting approach to generate an *Igh*–*Igk* hybrid locus in a single Jκ5 allele *v-Abl* line in which we had already deleted one copy of the entire *Igh* locus (Fig. 4a). In this line (*Igh*–*Igk* hybrid line), the targeted balanced translocation fused the entire *Igk* at a point just upstream of the distal Vκ segments to the downstream portion of *Igh*, starting 85 kb upstream of IGCR1, on a large der(12;6) fusion chromosome (Fig. 4a and Extended Data Fig. 4a,b). Upon G1 arrest and ectopic RAG expression, the *Igh*–*Igk* hybrid line underwent Vκ-to-Jκ joining similarly to its parental line (Extended Data Fig. 4c; compare with Fig. 4e), and the retained downstream portion of the *Igh* underwent normal levels and patterns of D-to-J_H joining[6,7] (Extended Data Fig. 4d). Thus, the V(D)J recombination activities of the *Igk*-RC and *Igh*-RC are maintained in the *Igh*–*Igk* hybrid line. To further test the *Igh*–*Igk* hybrid line, we used HTGTS-V(D)J-seq to assay for joining of the matched J_H-23RSSs with Vκ-12RSSs across the Vκ locus fused upstream of IGCR1. Remarkably, the J_H segments joined to both inversional- and deletional-oriented Vκ segments across the Vκ locus, which is in inverted orientation with respect to J_H-RSSs (Fig. 4b,c). Although the level of Vκ-to-J_H joining across the *Igh*–*Igk* hybrid locus was only 14% that of Vκ-to-Jκ joining in the normal *Igk* locus (Fig. 4b; compare with Fig. 2j total junction number), this level is far higher than that of residual V_H-to-DJ_H joining across an inverted V_H locus in bone marrow pro-B cells[7]. Notably, this long-range Vκ-to-J_H joining occurs in *v-Abl* cells, which have high levels of WAPL that essentially abrogate long-range V_H-to-DJ_H joining beyond low-level joining of the most proximal V_H segments[7]. Finally, the pattern of Vκ-to-J_H joining across the inverted Vκ locus was quite similar

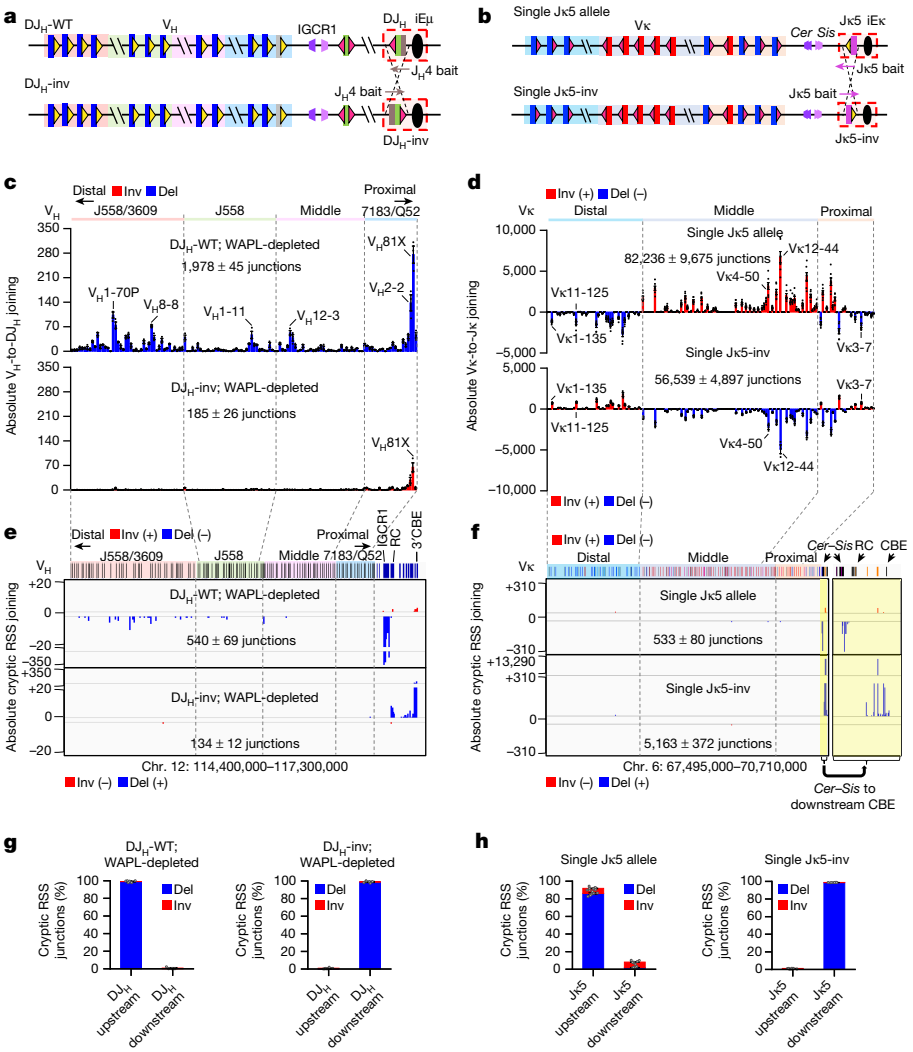

Fig. 3 | Inverting RC RSS orientation reverses RAG scanning direction and abrogates IgH, but not Igκ, V(D)J recombination. a, Diagram of pre-rearranged DQ52J_H4 in DJ_H-WT (top) and DJ_H-inv (bottom) WAPL-degron *v-Abl* lines. **b**, Diagram of Jκ5 in normal (top) and inverted (bottom) orientation from the single Jκ5 and single Jκ5-inv *v-Abl* lines. **c**, Absolute level of individual V_H usage from DJ_H-WT (top) and DJ_H-inv (bottom) lines with WAPL depletion. **d**, Absolute level of individual Vκ usage from the single Jκ5 allele (top) and single Jκ5-inv (bottom) lines. **e**, Absolute level of pooled RAG off-target junctions from three repeats in the *Igh* locus from DJ_H-WT (top) and DJ_H-inv (bottom) lines with WAPL depletion. **f**, Absolute level of pooled RAG off-target junctions from three repeats in the *Igk* locus from the single Jκ5 (top) and single Jκ5-inv (bottom) lines. RAG off-target junction profiles downstream of the *Igk* locus from *Cer* to the downstream CBE are enlarged on the right. The single Jκ5 allele data (**d**,**f**, top) are the same as those shown in Fig. 2f,g; but are plotted here as absolute levels rather than percentages for better alignment and comparison with results from the single Jκ5-inv line. **g**, Percentage of inversional (red) and deletional (blue) cryptic RSS junctions within indicated DJ_H upstream (chr. 12:114,666,726–117,300,000) and downstream (chr. 12:114,400,000–114,666,725) region from the DJ_H-WT (left) and DJ_H-inv (right) lines with WAPL depletion. **h**, Percentage of inversional (red) and deletional (blue) cryptic RSS junctions within indicated Jκ5 upstream (chr. 6:67,495,000–70,674,000) and downstream (chr. 6: 70,674,001–70,710,000) region from the single Jκ5 allele (left) and single Jκ5-inv (right) lines. Data are presented as mean ± s.e.m. from 3 (**c**,**g**), 7 (**d**, top, **h**, left) or 4 (**d**, bottom, **h**, right) biological repeats.

to that of Jκ joining to an inverted Vκ locus, with Vκ1-135 dominating rearrangement (Fig. 4c; compare with Fig. 2j).

For further comparison of Vκ-to-J_H rearrangement patterns and levels, we used a CRISPR–Cas9 approach to modify the *Igh–Igk* hybrid locus by first inverting the Vκ locus, so that it is in the same relative orientation to J_H-RSSs as the normal Vκ locus is to Jκ-RSSs (Extended Data Fig. 5a). To avoid potential confounding effects of competing D-to-J_H rearrangements, we deleted all D segments upstream of DQ52 and inactivated both DQ52 RSSs by targeted mutation (Extended Data Fig. 5a), leaving inactivated DQ52 in its normal position to retain its germline promoter and transcription to contribute to *Igh*-RC activity[29]. This further modified *v-Abl* line was termed the '*Igh–Igk* hybrid-Vκ line' (Extended Data Fig. 5a). HTGTS-V(D)J-seq analyses of Vκ-to-J_H joining in the *Igh–Igk* hybrid-Vκ line revealed J_H joining to both deletional- and inversional-oriented Vκ segments across the locus, but at approximately 9% the level of bona fide Vκ-to-Jκ5 joins (Extended Data Fig. 5b–d; compare with Fig. 4e). Whereas the joining patterns of middle and distal Vκ segments were very similar to those of the normal locus, relative utilization of the proximal deletional-oriented Vκ segments was increased (Extended Data Fig. 5d; compare with Fig. 4e). The increased proximal Vκ utilization phenotype could potentially reflect leakiness of the IGCR1 scanning impediment, enabling low-level RAG linear scanning to pass into the proximal Vκ locus versus the *Igh* locus in which IGCR1 is backed up by proximal V_H-associated CBE impediments[16,26]. To test this possibility, we compared Vκ rearrangement patterns of the *Igh–Igk* hybrid-Vκ line to those of single Jκ5 lines in which either *Cer*, *Sis* or both *Cer* and *Sis* were deleted (Extended Data Fig. 6). Consistent with prior analyses[12,30], *Cer* alone maintained nearly wild-type joining

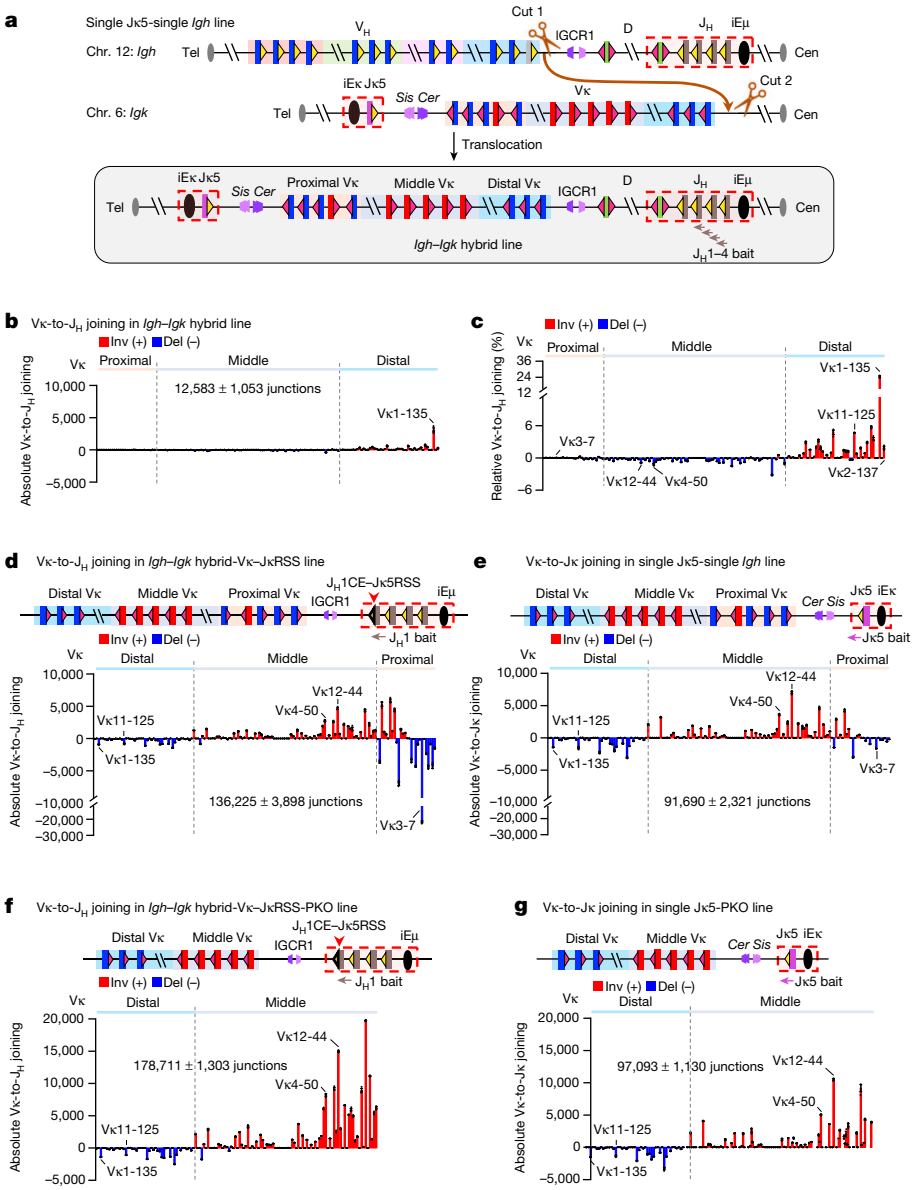

Fig. 4 | RSS replacements in *Igh–Igk* hybrid loci demonstrate superior strength of *Igk*-RSSs versus *Igh*-RSSs. a, Strategy for generating a targeted chromosomal translocation between chr. 12 and chr. 6 in the single Jκ5-single *Igh v-Abl* line. Cut 1 and Cut 2 show the locations of two single guide RNAs (sgRNAs) used for targeting. **b**,**c**, Absolute level (**b**) and relative percentage (**c**) of individual Vκ-to-$J_H$joins in the *Igh–Igk* hybrid line with J_H1-4 bait. The patterns of Vκ usage in **c** and Fig. 2j are highly similar (two-sided Pearson's $r = 0.98$, $P = 9.6 \times 10^{-110}$). **d**, Absolute level of individual Vκ-to-$J_H$joins in the *Igh–Igk* hybrid-Vκ-JκRSS line in which J_H1-23RSS was replaced with a Jκ5-23RSS, assayed with J_H1 bait. The patterns of Vκ usage in **d** and Extended Data Fig. 5d are highly similar (two-sided Pearson's $r = 0.89$, $P = 1.6 \times 10^{-56}$), but total rearrangement level in **d** is 17-fold higher than that in Extended Data Fig. 5c ($P = 0.0007$; unpaired, two-sided Welch's *t*-test). Note that Vκ3-7 is highly over-utilized, perhaps promoted by its closely associated E2A site (Supplementary Data 1). **e**, Absolute level of individual Vκ-to-Jκ joins in the single Jκ5-single *Igh* line with Jκ5 bait. **f**, Absolute level of individual Vκ-to-$J_H$joins in the *Igh–Igk* hybrid-Vκ-JκRSS-PKO line in which proximal Vκ domain was deleted, assayed with J_H1 bait. **g**, Absolute level of individual Vκ-to-Jκ joins in the single Jκ5-PKO line with Jκ5 bait. The patterns of Vκ usage in **f**,**g** are highly similar (two-sided Pearson's $r = 0.90$, $P = 1.2 \times 10^{-49}$). Vκ utilization data are presented as mean ± s.e.m. from 3 biological repeats.

patterns, whereas the absence of both *Cer* and *Sis* greatly increased proximal Vκ rearrangements at the expense of distal Vκ rearrangements (Extended Data Fig. 6e,f). *Cer* and *Sis* deletion also led to extended linear RAG scanning from the ectopic primary *Igk*-RC into the proximal Vκ region (Extended Data Fig. 6g–j). Notably, the rearrangement patterns in cells with *Sis* alone in which *Cer* was deleted were remarkably similar to those of the *Igh–Igk* hybrid-Vκ line (compare Extended Data Fig. 6a,c). Together, these results support the notion that relative leakiness of the IGCR1 CBE-based impediment, as compared to *Cer–Sis* deletion, results in increased utilization of proximal Vκ segments in the *Igh–Igk* hybrid-Vκ line. Finally, 3C-HTGTS analyses of the hybrid locus confirmed both the greater strength of the *Cer–Sis* anchor compared with IGCR1 and the relative weakness of Vκ locus loop extrusion impediments compared with those of the V_H locus (Extended Data Fig. 7).

As nearly all Vκ segments show low-level rearrangement to J_H segments in the presence of IGCR1, a candidate element that could enhance diffusional capture by the *Igh*-RC would be the Vκ-associated RSSs; which could, in theory, mediate this activity by being stronger than V_H-RSSs. In this regard, proximal V_H RSSs appear very weak in promoting V_H-to-DJ_H joining in the absence of directly associated CBEs

that increase their interaction with the *Igh*-RC[3]. This model leads to the further hypothesis that a potential limiting factor for the overall level of Vκ-to-J_H joins versus Vκ-to-Jκ joins, is relative strength of the Jκ-RSSs versus J_H-RSSs. To test this possibility, we further modified the *Igh*–*Igk* hybrid-Vκ locus by replacing J_H1-23RSS with Jκ5-23RSS to generate the '*Igh*–*Igk* hybrid-Vκ-JκRSS' line (Extended Data Fig. 5a), in which the entire downstream *Igh* locus including IGCR1, the *Igh*-RC and downstream sequences were in the same position as in the *Igh*–*Igk* hybrid-Vκ line. Remarkably, the pattern of Vκ-to-J_H rearrangements in the *Igh*–*Igk* hybrid-Vκ-JκRSS line was very similar to that of the parental *Igh*–*Igk* hybrid-Vκ line (Fig. 4d; compare with Extended Data Fig. 5d), but the absolute level of rearrangements to Vκ segments across the locus increased approximately 17-fold (compare Fig. 4d with Extended Data Fig. 5c) to levels slightly higher than those of Vκ-to-Jκ joining in the single Jκ5-single *Igh* line (Fig. 4e). To eliminate the dominance of Vκ3-7 (Fig. 4 caption) and, to a lesser extent, other proximal Vκ segments associated with leaky direct scanning through IGCR1 in the *Igh*–*Igk* hybrid-Vκ-JκRSS line, we deleted the most proximal deletional and inversional Vκ segments from this line to generate the '*Igh*–*Igk* hybrid-Vκ-JκRSS-PKO' line (Extended Data Fig. 5a). Of note, the pattern of Vκ-to-J_H rearrangements in the *Igh*–*Igk* hybrid-Vκ-JκRSS-PKO line was very similar to that in the single Jκ5 line with the same proximal Vκ deletion (single Jκ5-PKO line; Fig. 4f,g), with the absolute level of Vκ rearrangements across the *Igh*–*Igk* hybrid-Vκ-JκRSS-PKO locus approximately twofold higher than that of the single Jκ5-PKO line (Fig. 4f,g). Finally, to further test the relative RSS strength model, we performed the reciprocal experiment of replacing the Jκ5-23RSS with a J_H1-23RSS in the single Jκ5 allele *v-Abl* line (Extended Data Fig. 5e). Indeed, the J_H1-RSS supported only low-level Vκ-to-Jκ joining (1% the level supported by the Jκ5-RSS) (Extended Data Fig. 5f; compare with Fig. 4e), but essentially all Vκ segments were utilized (Extended Data Fig. 5g). The findings from our hybrid locus experiments demonstrate that strong *Igk*-RSSs are the major determinant of why *Igk*, but not *Igh*, supports robust diffusion-mediated V(D)J recombination.

Igk-RSSs are much stronger than *Igh*-RSSs

To directly test relative strength of *Igh* D-12RSSs versus that of a Vκ-12RSS in the context of short-range diffusional joining to the Jκ5-based RC, we used a CRISPR–Cas9-mediated approach to further modify the *Igh*–*Igk* hybrid locus. Specifically, we generated a deletion from 5,123 bp upstream of *Cer* (just downstream of the Vκ locus) to a point 453 bp upstream of DFL16.1 in the *Igh*–*Igk* hybrid locus to generate the '*Igh*–*Igk* hybrid-D-J_H' line (Extended Data Fig. 8a). In this line, the downstream portion of *Igk* including the Jκ5-based RC and *Cer*–*Sis* elements were placed just upstream of the DFL16.1, the 12 downstream D segments, and the J_H-RC (Extended Data Fig. 8a). We first assayed for D-to-J_H rearrangements in the *Igh*–*Igk* hybrid-D-J_H line and found the vast majority to be deletional and mostly utilize DFL16.1 and DQ52 (Extended Data Fig. 8b,c), similar to normal deletional-dominated patterns (Extended Data Fig. 4d). We also found D-to-Jκ5 rearrangements at much lower levels; but, nearly all were inversional to DQ52 and DFL16.1 (Extended Data Fig. 8d), consistent with Jκ-RC-bound RAG accessing these D segments by short-range diffusion across *Cer*–*Sis*, which is dominated by their stronger downstream D-RSSs[5]. Indeed, for D-to-J_H joining, the various D downstream RSSs are stronger than their upstream RSSs, with the DQ52 downstream RSS being the strongest[5]. To develop a line for directly comparing relative ability of a Vκ-RSS versus D-RSSs to mediate D-to-Jκ rearrangements, we deleted all J_H segments from the *Igh*–*Igk* hybrid-D-J_H line to generate the '*Igh*–*Igk* hybrid-D' line (Fig. 5a and Extended Data Fig. 8a). Activation of V(D)J recombination in this line resulted in primarily DQ52 joining to Jκ5 in which the strong downstream DQ52-RSS dominated rearrangements that were predominantly (13-fold) inversional versus deletional (Fig. 5a). Again, the high level of inversional DQ52-to-Jκ5 joining is consistent with short-range diffusional access across *Cer*–*Sis*. Remarkably, replacement of the weaker upstream DQ52-12RSS with the 12RSS of the highly utilized Vκ12-44 in the *Igh*–*Igk* hybrid-D line led to a 114-fold increase in the level of Jκ5 deletional joining to DQ52 (Fig. 5b; compare with Fig. 5a), a level approximately 26-fold greater than that of inversional joining mediated by the downstream DQ52-RSS (Fig. 5b). These results demonstrate the remarkable functional strength of the Vκ-12RSS, compared with the DQ52 downstream 12RSS and all other *Igh* D-12RSSs in mediating diffusion-based D-to-Jκ5 rearrangements.

Igk-RSSs programme diffusional joining in *Igh*

We tested the relative ability of the frequently utilized Vκ11-125 RSS versus that of the upstream DQ52-RSS to mediate joining of proximal V_H segments to the inverted DQ52J_H4-based RC. For this experiment, we did not deplete WAPL to leave IGCR1 CBE impediments fully functional to enforce short-range diffusion mediated joining of the most proximal V_H segments. With high WAPL levels, distal V_H segments are prevented from being extruded past IGCR1 by many robust CBE impediments associated with proximal and middle V_H-RSSs[6,26,27] (Extended Data Fig. 7b). In the DQ52J_H4-inverted line, we found very low levels of inversional joining to proximal V_H5-2 mediated by the inverted upstream DQ52-12RSS (Fig. 5c). However, upon replacement of this DQ52-12RSS with the Vκ11-125-12RSS, inversional rearrangements increased approximately 13-fold, predominantly to V_H5-2 but at lower levels to additional proximal V_H segments (Fig. 5d; compare with Fig. 5c). To test the cooperative ability of *Igk*-RSSs to promote inversional rearrangement, we replaced the V_H5-2-23RSS with the Jκ1-23RSS in the *v-Abl* line in which the DQ52-12RSS was replaced with the Vκ11-125-12RSS. Remarkably, the Jκ1-RSS replacement led to a further 35-fold increase in V_H5-2 to inverted DQ52J_H4 joining (Fig. 5e; compare with Fig. 5d). Indeed, the overall increase in V_H5-2 to inverted DQ52J_H4 joining was more than 380-fold (Fig. 5e; compare with Fig. 5c). This joining level approaches that of direct deletional V_H5-2-to-DFL16.1J_H4 joining in the absence of IGCR1[3]. Together, these findings demonstrate that paired *Igk* 12 and 23 RSSs programme the *Igh* to undergo robust V_H-to-DJ_H inversional joining mediated by short-range diffusion.

Relevance of RSS RIC scores to joining mechanism

The theoretical strength of given 12RSSs and 23RSSs, respectively, has been estimated on the basis of an algorithm that assesses recombination information content (RIC) scores of their sequence[31–33]. Previous studies failed to detect strong correlations between RIC scores of V_H-RSSs or, to a lesser extent, Vκ-RSSs and their utilization frequency[34–37]. Predicted RIC thresholds for 12RSSs and 23RSSs are −38.81 and −58.45, respectively[31,33], with increasing RIC scores proposed to reflect increasing RSS strength. Because 12RSS and 23RSS RIC scores cannot be directly compared[31,32], we examined Vκ-12RSS or V_H-23RSS RIC scores and corresponding Vκ or V_H usage in, respectively, single Jκ5 allele *v-Abl* cells to focus on primary Vκ rearrangements, or normal pro-B cells to focus on V_H rearrangements in the context of physiological WAPL down-regulation[7]. Most highly used Vκ-12RSSs in single Jκ5 allele *v-Abl* cells have RIC scores tightly clustered between −16 and −8, with −8 being the highest observed (Fig. 5f); Vκ-12RSSs with RICs below −20 are rarely utilized (Fig. 5f). Similar results were observed in single Jκ1 *v-Abl* cells (Extended Data Fig. 8e). Approximately 26% of Vκ-RSSs with high RIC scores are rarely utilized. The reason for this is unknown; but one possibility is that these Vκ segments are not in chromatin regions that promote sufficient accessibility to the RAG-bound RC[36,37]. V_H-23RSSs, which span a broader range of RIC scores from −57 to −16, support a similar range of utilization levels, with the exception of proximal V_H5-2 and V_H2-2 that have lower RIC scores but very high utilization (Fig. 5g). But, robust rearrangement of these two V_H segments is promoted by CBEs within 20 bp of their RSSs, which promotes accessibility by enhancing

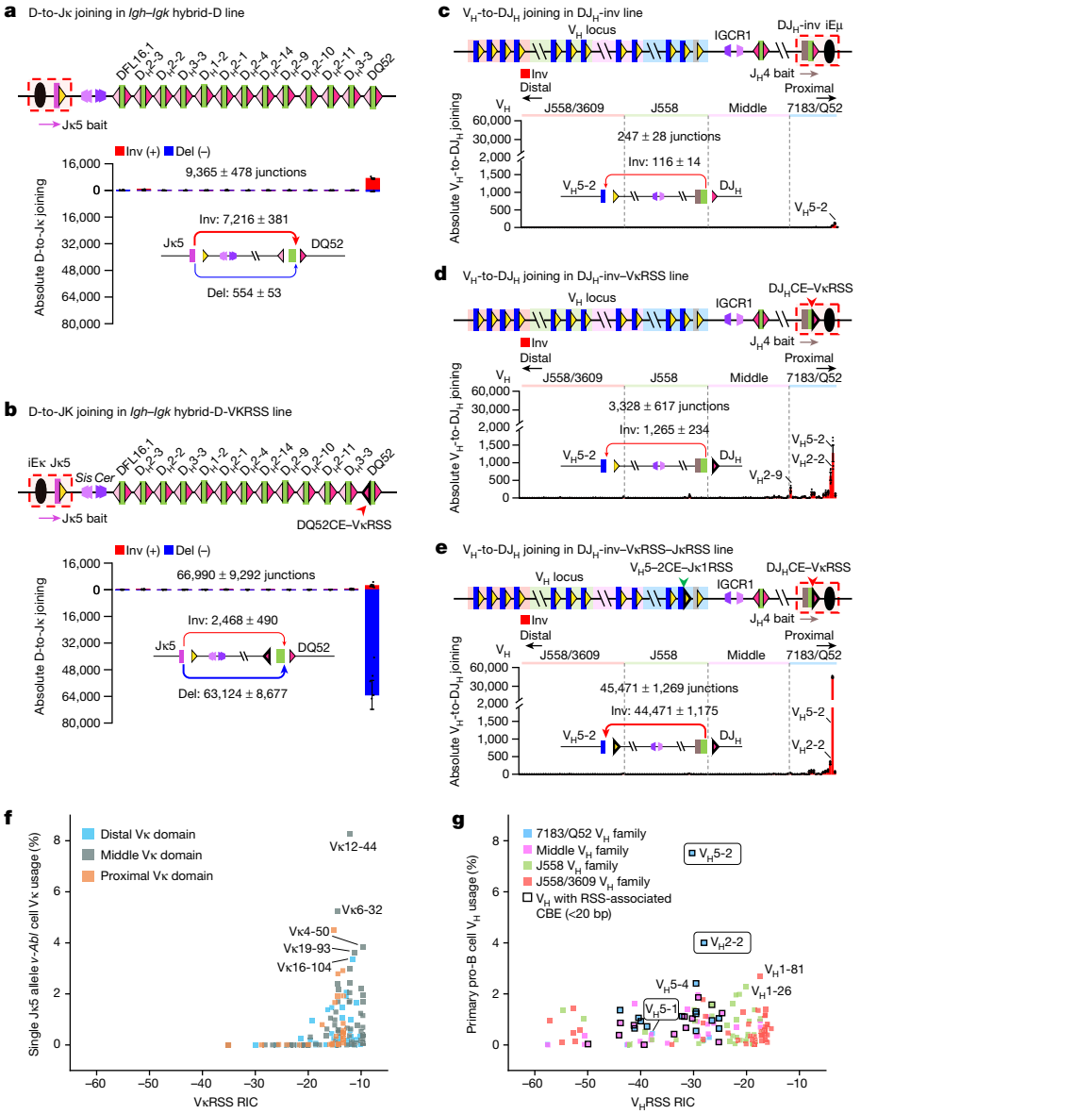

Fig. 5 | *Igk*-RSSs enhance diffusional D-to-Jκ joining in the *Igh–Igk* hybrid locus and activate inversional V_H-to-DJ_H joining in the *Igh* locus. a,**b**, Absolute level of individual D-to-Jκ joins in the *Igh–Igk* hybrid-D line (**a**) and the *Igh–Igk* hybrid-D-VκRSS line in which the DQ52 upstream 12RSS was replaced with a Vκ12-44 12RSS (**b**), assayed with Jκ5 bait. Deletional DQ52-to-Jκ5 joining in **b** is 114-fold higher than that in **a** ($P = 0.0008$). **c**–**e**, Absolute level of individual inversional V_H-to-DJ_H joins in the DJ_H-inv line (**c**), the DJ_H-inv-VκRSS line, in which DQ52 upstream 12RSS was replaced with a Vκ11-125 12RSS (**d**) and the DJ_H-inv-VκRSS-JκRSS line, in which V_H5-2 23RSS was replaced with a Jκ1-23RSS (**e**), assayed with J_H4 bait. Total rearrangement level in **d** is 13-fold higher than that in **c** ($P = 0.0153$). Inversional V_H5-2 usage level in **e** is 35-fold higher than that in **d** ($P = 0.0005$) and 383-fold higher than that in **c** ($P = 0.0007$). In **a**–**e**, red arrows show inversional joins and blue arrows show deletional joins. Corresponding junction numbers are shown. Arrow thickness represents relative amounts of junctions. **f**, Comparison of relative Vκ usage in the single Jκ5 allele *v-Abl* cells with Vκ-RSS RIC scores calculated using the Recombination Signal Sequences Site[33] (http://www.itb.cnr.it/rss). Vκ segments are colour-coded according to the three Vκ domains with names indicated for highly used Vκ segments. **g**, Comparison of relative V_H usage in primary pro-B cells[7] with V_H-RSS RIC scores. V_H segments are colour-coded according to the four V_H domains, and square black outlines indicate V_H segments with CBEs within 20 bp of their RSSs. The circled V_H5-1, V_H5-2 and V_H2-2 have been shown to depend on associated CBEs for robust utilization[3]. D and V_H utilization data are presented as mean ± s.e.m. from 4 (**a**,**d**), 6 (**b**) and 3 (**c**,**e**) biological repeats. *P* values were calculated with unpaired, two-sided Welch's *t*-test.

V_H-RSS contact with the RC during RAG scanning[3]. Indeed, inactivation of these RSS-associated CBEs reduces utilization to near baseline, consistent with RSSs themselves being very weak[3]. Likewise, adding an associated CBE to the barely utilized, low RIC score proximal V_H5-1 RSS makes it the most highly utilized[3]. Transcriptional impediments are likely to function similarly for more distal V_H-RSSs[5–7]; although more distal V_H-RSSs also have higher RIC scores (Fig. 5g). Notably, 28 of the most proximal V_H segments have CBEs within 20 bp of their RSSs; but, none of the 103 Vκ segments are associated with such proximal CBEs[37].

Discussion

The molecular basis by which *Igk*, but not *Igh*, is able to utlilize a diffusion-based mechanism to promote both deletional and inversional joining was a long-standing mystery. Our studies reveal that *Igk* and *Igh* evolved RSSs with distinctly different strength to carry out their distinct mechanisms of long-range V(D)J recombination. Until now, RSSs were not known to function in the broad context of mediating distinct V(D)J recombination mechanisms between loci.

Long ago, we found that differential RSS strength mediates ordered Dβ-to-Jβ and Vβ-to DJβ joining by a "beyond 12/23" mechanism[38,39]; and, more recently, weaker Vβ-RSSs were implicated in facilitating allelic exclusion of Vβ-to-DJβ joining[40]. *Igh* DQ52 evolved a relatively strong downstream RSS to enforce deletional joining to closely linked J_H-RSSs via short-range diffusion; correspondingly, when inverted the strong downstream DQ52-RSS mediates robust inversional joining[5]. Yet, insertion of an inverted DQ52 in an upstream position beyond diffusion range led the weaker upstream DQ52-RSS—now facing downstream—to dominantly generate deletional rearrangements to J_H via linear RAG scanning[5]. The relative strength of *Igk*-RSSs is underscored by our finding that a Vκ-12RSS is orders of magnitude stronger than the downstream DQ52-12RSS in mediating diffusional joining in the context of the *Cer–Sis* impediment. Similarly, whereas *Igh* IGCR1 is weaker in impeding RAG scanning than *Cer–Sis*, in the *Igh–Igk* hybrid-Vκ locus, it supports substantial diffusional Vκ capture and joining by RAG bound to a downstream *Igh*-RC in which the J_H-RSS is replaced with a Jκ-RSS. Moreover, robust diffusional joining of V_H to an inverted DJ_H-RC occurs only when V_H-RSS and DJ_H-RSS are replaced with 12/23-matched *Igk*-RSSs. Whereas single Vκ- or Jκ-RSSs increase diffusion-mediated joining in the above contexts, highly robust joining occurs only with 12/23 matched *Igk*-RSSs, either through multiplicative effects and/or by more robust pairing. In summary, our findings indicate that the *Igk* evolved both a robust *Cer* diffusion platform and strong RSSs that function robustly in the context of more transient RC interactions that likely occur during diffusion-mediated primary Vκ-to-Jκ joining (Extended Data Fig. 9). By contrast, weak *Igh*-RSSs and a less robust IGCR1 impediment probably evolved to facilitate mediation of V_H utilization by WAPL down-regulated modulation of scanning impediments during long-range linear RAG scanning. Finally, our studies suggest the testable hypothesis that *Igk* secondary rearrangements with *Cer–Sis* deleted or displaced occur by linear RAG scanning.

Online content

Any methods, additional references, Nature Portfolio reporting summaries, source data, extended data, supplementary information, acknowledgements, peer review information; details of author contributions and competing interests; and statements of data and code availability are available at https://doi.org/10.1038/s41586-024-07477-y.

1. Schatz, D. G. & Swanson, P. C. V(D)J recombination: mechanisms of initiation. *Annu. Rev. Genet.* **45**, 167–202 (2011).
2. Zhang, Y., Zhang, X., Dai, H.-Q., Hu, H. & Alt, F. W. The role of chromatin loop extrusion in antibody diversification. *Nat. Rev. Immunol.* **22**, 550–566 (2022).
3. Jain, S., Ba, Z., Zhang, Y., Dai, H.-Q. & Alt, F. W. CTCF-binding elements mediate accessibility of RAG substrates during chromatin scanning. *Cell* **174**, 102–116.e14 (2018).
4. Hu, J. et al. Chromosomal loop domains direct the recombination of antigen receptor genes. *Cell* **163**, 947–959 (2015).
5. Zhang, Y. et al. The fundamental role of chromatin loop extrusion in physiological V(D)J recombination. *Nature* **573**, 600–604 (2019).
6. Ba, Z. et al. CTCF orchestrates long-range cohesin-driven V(D)J recombinational scanning. *Nature* **586**, 305–310 (2020).
7. Dai, H.-Q. et al. Loop extrusion mediates physiological Igh locus contraction for RAG scanning. *Nature* **590**, 338–343 (2021).
8. de Almeida, C. R., Hendriks, R. W. & Stadhouders, R. Dynamic control of long-range genomic interactions at the immunoglobulin κ light-chain locus. *Adv. Immunol.* **128**, 183–271 (2015).
9. Collins, A. M. & Watson, C. T. Immunoglobulin light chain gene rearrangements, receptor editing and the development of a self-tolerant antibody repertoire. *Front. Immunol.* **9**, 2249 (2018).
10. Nemazee, D. Mechanisms of central tolerance for B cells. *Nat. Rev. Immunol.* **17**, 281–294 (2017).
11. Xiang, Y., Zhou, X., Hewitt, S. L., Skok, J. A. & Garrard, W. T. A multifunctional element in the mouse Igκ locus that specifies repertoire and Ig loci subnuclear location. *J. Immunol.* **186**, 5356–5366 (2011).
12. Xiang, Y., Park, S.-K. & Garrard, W. T. Vκ gene repertoire and locus contraction are specified by critical DNase I hypersensitive sites within the Vκ–Jκ Intervening region. *J. Immunol.* **190**, 1819–1826 (2013).
13. Ru, H. et al. Molecular mechanism of V(D)J recombination from synaptic RAG1–RAG2 complex structures. *Cell* **163**, 1138–1152 (2015).
14. Kim, M.-S. et al. Cracking the DNA code for V(D)J recombination. *Mol. Cell* **70**, 358–370. e4 (2018).
15. Gauss, G. H. & Lieber, M. R. The basis for the mechanistic bias for deletional over inversional V(D)J recombination. *Genes Dev.* **6**, 1553–1561 (1992).
16. Guo, C. et al. CTCF-binding elements mediate control of V(D)J recombination. *Nature* **477**, 424–430 (2011).
17. Hill, L. et al. *Wapl* repression by Pax5 promotes *V* gene recombination by *Igh* loop extrusion. *Nature* **584**, 142–147 (2020).
18. Yamagami, T., ten Boekel, E., Andersson, J., Rolink, A. & Melchers, F. Frequencies of multiple IgL chain gene rearrangements in single normal or $κ_L$ chain–deficient B lineage cells. *Immunity* **11**, 317–327 (1999).
19. Lin, W. C. & Desiderio, S. Cell cycle regulation of V(D)J recombination-activating protein RAG-2. *Proc. Natl Acad. Sci. USA* **91**, 2733–2737 (1994).
20. Bredemeyer, A. L. et al. ATM stabilizes DNA double-strand-break complexes during V(D)J recombination. *Nature* **442**, 466–470 (2006).
21. Lin, S. G. et al. Highly sensitive and unbiased approach for elucidating antibody repertoires. *Proc. Natl Acad. Sci. USA* **113**, 7846–7851 (2016).
22. Moore, M. W., Durdik, J., Persiani, D. M. & Selsing, E. Deletions of kappa chain constant region genes in mouse lambda chain-producing B cells involve intrachromosomal DNA recombinations similar to V–J joining. *Proc. Natl Acad. Sci. USA* **82**, 6211–6215 (1985).
23. Hill, L. et al. Igh and Igk loci use different folding principles for V gene recombination due to distinct chromosomal architectures of pro-B and pre-B cells. *Nat. Commun.* **14**, 2316 (2023).
24. Barajas-Mora, E. M. et al. A B-cell-specific enhancer orchestrates nuclear architecture to generate a diverse antigen receptor repertoire. *Mol. Cell* **73**, 48–60 (2019).
25. Barajas-Mora, E. M. et al. Enhancer-instructed epigenetic landscape and chromatin compartmentalization dictate a primary antibody repertoire protective against specific bacterial pathogens. *Nat. Immunol.* **24**, 320–336 (2023).
26. Liang, Z. et al. Contribution of the IGCR1 regulatory element and the 3′Igh CTCF-binding elements to regulation of Igh V(D)J recombination. *Proc. Natl Acad. Sci. USA* **120**, e2306564120 (2023).
27. Dai, H.-Q. et al. Loop extrusion mediates physiological locus contraction for V(D)J recombination. Preprint at *bioRxiv* https://doi.org/10.1101/2020.06.30.181222 (2020).
28. Bevington, S. & Boyes, J. Transcription-coupled eviction of histones H2A/H2B governs V(D)J recombination. *EMBO J.* **32**, 1381–1392 (2013).
29. Nitschke, L., Kestler, J., Tallone, T., Pelkonen, S. & Pelkonen, J. Deletion of the DQ52 element within the Ig heavy chain locus leads to a selective reduction in VDJ recombination and altered D gene usage. *J. Immunol.* **166**, 2540–2552 (2001).
30. Xiang, Y., Park, S.-K. & Garrard, W. T. A major deletion in the Vκ–Jκ intervening region results in hyper-elevated transcription of proximal Vκ genes and a severely restricted repertoire. *J. Immunol.* **193**, 3746–3754 (2014).
31. Cowell, L. G., Davila, M., Kepler, T. B. & Kelsoe, G. Identification and utilization of arbitrary correlations in models of recombination signal sequences. *Genome Biol.* **3**, research0072.1 (2002).
32. Cowell, L. G., Davila, M., Yang, K., Kepler, T. B. & Kelsoe, G. Prospective estimation of recombination signal efficiency and identification of functional cryptic signals in the genome by statistical modeling. *J. Exp. Med.* **197**, 207–220 (2003).
33. Merelli, I. et al. RSSsite: a reference database and prediction tool for the identification of cryptic Recombination Signal Sequences in human and murine genomes. *Nucleic Acids Res.* **38**, W262–W267 (2010).
34. Choi, N. M. et al. Deep sequencing of the murine Igh repertoire reveals complex regulation of nonrandom V gene rearrangement frequencies. *J. Immunol.* **191**, 2393–2402 (2013).
35. Bolland, D. J. et al. Two mutually exclusive local chromatin states drive efficient V(D)J recombination. *Cell Rep.* **15**, 2475–2487 (2016).
36. Matheson, L. S. et al. Local chromatin features including PU.1 and IKAROS binding and H3K4 methylation shape the repertoire of immunoglobulin kappa genes chosen for V(D)J recombination. *Front. Immunol.* **8**, 1550 (2017).
37. Kleiman, E., Loguercio, S. & Feeney, A. J. Epigenetic enhancer marks and transcription factor binding influence Vκ gene rearrangement in pre-B cells and pro-B cells. *Front. Immunol.* **9**, 2074 (2018).
38. Bassing, C. H. et al. Recombination signal sequences restrict chromosomal V(D)J recombination beyond the 12/23 rule. *Nature* **405**, 583–586 (2000).
39. Wu, C. et al. Dramatically increased rearrangement and peripheral representation of Vβ14 driven by the 3′Dβ1 recombination signal sequence. *Immunity* **18**, 75–85 (2003).
40. Wu, G. S. et al. Poor quality Vβ recombination signal sequences stochastically enforce TCRβ allelic exclusion. *J. Exp. Med.* **217**, e20200412 (2020).

Methods

Experimental procedures

Statistical methods were not used to predetermine sample size. Experiments were not randomized. Investigators were not blinded to allocation during experiments and outcome assessment.

Mice

Wild-type 129SV mice were purchased from Taconic Biosciences. All mouse work was performed in compliance with all the relevant ethical regulations established by the Institutional Animal Care and Use Committee (IACUC) of Boston Children's Hospital and under protocols approved by the IACUC of Boston Children's Hospital. Mice were maintained on a 14-h light/10-h dark schedule in a temperature (22 ± 3 °C) and humidity (35% ~ 70% ± 5%)-controlled environment, with food and water provided ad libitum. Male and female mice were used equally for all experiments.

Generation and characterization of the entire Vκ locus inversion mouse model

The CRISPR–Cas9-mediated entire Vκ locus inversion modifications were made on one *Igk* allele in the TC1 embryonic stem (ES) cell line. Targeting of the ES cells was performed using sgRNA1 and sgRNA2 as previously described[41]. Positive clones with 3.1 Mb Vκ locus inversion were identified by PCR and confirmed by Sanger sequencing. After testing negative for mycoplasma, the ES clone with Vκ inversion was injected into RAG2-deficient blastocysts to generate chimeras[42]. The chimeric mice were bred with wild-type 129SV mice for germline transmission of the targeted inversion, and bred to homozygosity. Sequences of all sgRNAs and oligonucleotides mentioned in this section and sections below are listed in Supplementary Table 1.

Generation of V_H7-3 *Igh* pre-rearranged; *Rag2*$^{-/-}$ mouse model

The heterozygous or homozygous V_H7-3 *Igh* pre-rearranged mice (V_H7-3$^{wt/re}$ or V_H7-3$^{re/re}$) were generated through induced pluripotent stem (iPS) cells and maintained in the Alt laboratory. To perform 3C-HTGTS experiments with RAG2-deficient background, V_H7-3$^{wt/re}$ or V_H7-3$^{re/re}$ mice were crossed with *Rag2*$^{-/-}$ mice to obtain V_H7-3$^{wt/re}$; *Rag2*$^{-/-}$ or V_H7-3$^{re/re}$; *Rag2*$^{-/-}$ mice on the 129SV background.

Purification of bone marrow precursor B cells

For RAG on-target and off-target analysis, single cell suspensions were derived from bone marrows of 4- to 6-week-old male and female wild-type and *Igk* Vκ locus inversion 129SV mice and incubated in Red Blood Cell Lysing Buffer (Sigma-Aldrich, R7757) to deplete the erythrocytes. B220^{+}CD43^{low}IgM^{-} pre-B cells were isolated by staining with anti-B220–APC (1:1,000 dilution; eBioscience, 17-0452-83), anti-CD43–PE (1:400 dilution; BD Biosciences, 553271) and anti-IgM–FITC (1:500 dilution; eBioscience, 11-5790-81) and purifying via fluorescence-activated cell sorting (FACS), and the purified primary pre-B cells were directly used for HTGTS-V(D)J-seq as described[21,43].

For 3C-HTGTS experiments, B220-positive primary pre-B cells were purified via anti-B220 MicroBeads (Miltenyi, 130-049-501) from 4- to 6-week-old male and female V_H7-3$^{wt/re}$; *Rag2*$^{-/-}$ or V_H7-3$^{re/re}$; *Rag2*$^{-/-}$ mice. Purified pre-B cells from 3 or 4 mice were pooled together for each 3C-HTGTS experiment. Each mouse was double-checked and confirmed by PCR and Sanger sequencing prior to various assays.

Generation of single Jκ5 *v-Abl* cell line and its derivatives

The construction of sgRNA–Cas9 plasmids and methods for nucleofection-mediated targeting experiments described for this section and all subsequent paragraphs describing *v-Abl* line modifications were performed as previously described[7]. All *v-Abl* cell lines have not been tested for mycoplasma contamination.

The initial 'parental' *Rag2*$^{-/-}$;*Eμ-Bcl2*$^{+}$ *v-Abl* cell line in the 129SV background was generated previously[6]. Random 1–4 bp indels (barcodes) were introduced into a site ~85 bp downstream of the Jκ5-RSS heptamer and ~40 bp upstream of the Jκ5 bait primer on both alleles in this parental line, similarly to the approach previously described to modify J_H4[6]. The resulting 'Jκ5-barcoded' *v-Abl* line was further targeted with sgRNA1 and sgRNA2 to invert the whole Vκ locus on one allele and leaving the other allele intact. Thus, the *Igk* allele-specific barcode permits the separation of sequencing reads derived from the wild-type allele and the Vκ inverted allele assayed with the same bait primer under the same cellular context. This barcoded line was used to generate the data in Fig. 1b,e.

To facilitate further modifications on the *Igk* locus, the Jκ5-barcoded *v-Abl* line was targeted with sgRNA1 and sgRNA3 that deleted the entire *Igk* locus on one allele and left the other allele intact. The barcode was not relevant to further studies based on this single *Igk* allele line or its derivatives. The single *Igk* allele line was further targeted by another two pairs of sgRNAs to separately delete Jκ1 to Jκ4 (sgRNA4 and sgRNA5) and downstream *Igk*-RS (sgRNA6 and sgRNA7) to exclude confounding secondary rearrangements and keep the configuration unchanged between Jκ5 and iEκ. This line is referred to as the 'single Jκ5 allele line'.

The single Jκ5 allele line was further modified by specifically designed Cas9–sgRNA to generate the single Jκ5-Vκ inv line (sgRNA8 and sgRNA9), single Jκ5-inv line (sgRNA10 and sgRNA11), single Jκ5-single *Igh* line (sgRNA12 and sgRNA13), single Jκ5-PKO line (sgRNA2 and sgRNA14), single Jκ5-*Cer* knockout (KO) line (sgRNA15 and sgRNA16), single Jκ5-*Sis* KO line (sgRNA17 and sgRNA18), and single Jκ5-*CerSis* KO line (sgRNA15 and sgRNA18).

The single Jκ1 allele *v-Abl* line was generated from the single *Igk* allele line by separately deleting Jκ2 to Jκ5 (sgRNA10 and sgRNA19) and deleting downstream *Igk*-RS (sgRNA6 and sgRNA7).

All candidate clones with desired gene modifications were screened by PCR and confirmed by Sanger sequencing.

Generation and analysis of DJ_H pre-rearranged WAPL-degron *v-Abl* cell lines

The DJ_H pre-rearranged *v-Abl* lines in C57BL/6 background were derived from the previously described WAPL-degron *v-Abl* line[7]. The open reading frame sequences of *Rag1* and *Rag2* were cloned into pMAX-GFP vector (Addgene, 177825) following the standard protocol to generate pMAX-Rag1 and pMAX-Rag2 plasmids. These two plasmids (each 2.5 μg) were nucleofected into 2.0×10^6 WAPL-degron *v-Abl* cells to allow endogenous D-to-J_H rearrangements mediated by transient RAG expression. Cells harbouring the desired DQ52J_H4 rearrangement (DJ_H-WT line) were subsequently identified by PCR screening and verified by Sanger sequencing. The DJ_H-inv *v-Abl* line was generated from the DJ_H-WT line by using Cas9–sgRNA to target sequences downstream of J_H4 and upstream of DQ52 (sgRNA20 and sgRNA21). The DJ_H-WT and DJ_H-inv lines were treated with IAA and Dox to deplete WAPL as described[7].

Generation of *Igh–Igk* hybrid *v-Abl* cell line and its derivatives

The *Igh–Igk* hybrid *v-Abl* cell line was derived from the single Jκ5 allele *v-Abl* line. In brief, the single Jκ5 allele line was targeted by sgRNA12 and sgRNA13 to generate the single Jκ5-single *Igh* line where the entire *Igh* locus was deleted from one allele. The single Jκ5-single *Igh* line was then targeted by sgRNA22 (cut 1, upstream of IGCR1 in *Igh*) and sgRNA8 (cut 2, upstream of Vκ2-137 in *Igk*) to generate a balanced chromosomal translocation between chromosomes 12 and 6. In the resulting *Igh–Igk* hybrid *v-Abl* line, the entire *Igk* locus along with the rest of chromosome 6 was appended onto chromosome 12 at a point upstream of IGCR1 in *Igh*, and the *Igh* V_H locus along with the small telomeric portion of chromosome 12 was reciprocally appended onto chromosome 6. To generate the *Igh–Igk* hybrid-Vκ line, the *Igh–Igk* hybrid line was sequentially modified to invert the entire Vκ locus (sgRNA15 and sgRNA23), mutate DQ52 RSSs (sgRNA24 and ssODN1) and delete all upstream D segments

(sgRNA25 and sgRNA26). To generate the *Igh–Igk* hybrid-Vκ-JκRSS-PKO line from the *Igh–Igk* hybrid-Vκ-JκRSS line, sgRNA2 and sgRNA14 were used to delete the proximal Vκ domain.

To generate the *Igh–Igk* hybrid-D-J_H line, the *Igh–Igk* hybrid line was targeted by sgRNA27 and sgRNA28 to delete IGCR1 and the entire Vκ locus. The *Igh–Igk* hybrid-D-J_H line was further modified to generate the *Igh–Igk* hybrid-D line where J_H1-4 has been deleted (sgRNA29 and sgRNA30).

All candidate clones with desired gene modifications were screened by PCR and confirmed by Sanger sequencing. See Fig. 4a and Extended Data Figs. 5a and 8a for detailed strategy and procedure.

Whole-chromosome painting

Whole-chromosome painting was performed on single Jκ5-single *Igh v-Abl* line and *Igh–Igk* hybrid *v-Abl* line using fluorescent probes tiling the entire chromosome 6 (Chr6-FITC, Applied Spectral Imaging) and chromosome 12 (Chr12-TxRed, Applied Spectral Imaging) according to standard protocol. In brief, cells were treated with colcemid at 0.05 μg ml^{-1} final concentration for 3 h before being processed for metaphase drop. The slides were dehydrated in ethanol series, denatured at 70 °C for 1.5 min, and hybridized to denatured probe mixture at 37 °C for 12–16 h. The slides were then washed, stained with DAPI, and imaged with Olympus BX61 microscope. ImageJ (1.53q) was used for image processing.

RSS replacement experiments

All RSS replacement modifications were generated via Cas9–sgRNA using short single-stranded DNA oligonucleotide (ssODN) as donor template. In brief, 2.5 μg Cas9–sgRNA plasmid and 5 μl 10 μM ssODN were co-transfected into 2.0×10^6 *v-Abl* cells. PCR screening was performed sequentially on pooled clones and then single clones, and subsequently verified by Sanger sequencing. Specifically, sgRNA31 and ssODN2 were used to replace J_H1-RSS with Jκ5-RSS in *Igh–Igk* hybrid-Vκ *v-Abl* line to generate the *Igh–Igk* hybrid-Vκ-JκRSS line; sgRNA32 and ssODN3 were used to replace Jκ5-RSS with J_H1-RSS in single Jκ5-single *Igh* line to generate the single Jκ5-single *Igh*-J_HRSS line; sgRNA33 and ssODN4 were used to replace DQ52 upstream RSS with Vκ12-44-RSS in *Igh–Igk* hybrid-D line to generate the *Igh–Igk* hybrid-D-VκRSS line; sgRNA34 and ssODN5 were used to replace DQ52 upstream RSS with Vκ11-125-RSS in DJ_H-inv line to generate the DJ_H-inv-VκRSS line; sgRNA35 and ssODN6 were used to replace V_H5-2-RSS with Jκ1-RSS in DJ_H-inv-VκRSS line to generate the DJ_H-inv-VκRSS-JκRSS line.

RAG complementation

RAG was reconstituted in RAG1-deficient *v-Abl* cells via retroviral infection with the pMSCV-RAG1-IRES-Bsr and pMSCV-Flag-RAG2-GFP vectors followed by 3–4 days of blasticidin (Sigma-Aldrich, 15205) selection to enrich for cells with virus integration[7]. RAG2 was reconstituted in RAG2-deficient *v-Abl* cells via retroviral infection with the pMSCV-Flag-RAG2-GFP vector followed by two days of puromycin (ThermoFisher, J67236) selection to enrich for cells with virus integration[5].

HTGTS-V(D)J-seq and data analyses

HTGTS-V(D)J-seq libraries were prepared as previously described[6,7,21,43] with 0.5–2 μg of genomic DNA (gDNA) from sorted primary pre-B cells or 10 μg of gDNA from G1-arrested RAG-complemented RAG-deficient *v-Abl* cells. The final libraries were sequenced on Illumina NextSeq550 with control software (2.2.0) or NextSeq2000 with control software (1.5.0.42699) using paired-end 150-bp sequencing kit. HTGTS-V(D)J-seq libraries were processed via the pipeline described previously[43]. For *Igh* rearrangement analysis in DJ_H-WT and DJ_H-inv WAPL-degron *v-Abl* lines, the data were aligned to the mm9_DQ52J_H4 genome and analysed with all duplicate junctions included in the analyses as previously described[43]. For analysis in DJ_H-inv-VκRSS and DJ_H-inv-VκRSS-JκRSS *v-Abl* lines, the data were aligned to the mm9_DQ52J_H4_VκRSS genome. For all other rearrangement analysis, primary pre-B cells and *v-Abl* cells used are from 129SV background. Since there is almost no difference in the *Igk* locus between C57BL/6 and 129SV genomic backgrounds[44], the data were aligned to the AJ851868/mm9 hybrid (mm9AJ) genome[6] except: data from *Igh–Igk* hybrid-Vκ-JκRSS and *Igh–Igk* hybrid-Vκ-JκRSS-PKO *v-Abl* lines were aligned to the mm9AJ_J_H1toJκ5RSS genome, data from single Jκ5-single *Igh*-J_HRSS *v-Abl* line were aligned to the mm9AJ_Jκ5toJ_H1RSS genome, and data from *Igh–Igk* hybrid-D-VκRSS *v-Abl* line were aligned to the mm9AJ_DQ52uptoVκRSS genome. To show the absolute level of V(D)J recombination, each HTGTS-V(D)J-seq library was down-sampled to 500,000 total reads (junctions + germline reads); to show the relative Vκ usage pattern across the Vκ locus, individual Vκ usage levels were divided by the total Vκ usage level in each HTGTS-V(D)J-seq library to obtain the relative percentage. Such analyses are useful for examining effects of potential regulatory element mutations. For example, differences in absolute rearrangement levels between two samples with the same relative rearrangement patterns would reflect differences in RAG or RC activity without changes in long-range regulatory mechanisms[7,26].

RAG off-targets were extracted from corresponding normalized HTGTS-V(D)J-seq libraries by removing on-target junctions on bona fide RSSs. We noticed the remaining junctions in the *Igk* locus were skewed to a few very strong RSS sites, which represent unannotated bona fide RSSs not associated with functional Vκ segments. We eliminated these strong RSSs from our cryptic RSS analyses by filtering out RSS sites with a CAC and additional at least 9 bp matches to the remaining ideal heptamer AGTG and ideal nonamer ACAAAAACC in the context of a 12-or-23-bp spacer—that is, at most 4-bp mismatches to the ideal RSS site. In addition, because coding end junctions are processed and can spread across several bps beyond the CAC cleavage site[4], the new code has the advantage of collapsing these coding end junctional signals within 15 bp into one peak mapped to the CAC cleavage site for better visualization of off-target coding junction peaks. For visualization of the actual distribution of coding end junctions, one can reveal them through analysis with our prior pipeline. Details of both pipelines used are provided in Code availability. Junctions are denoted as deletional if the prey cryptic RSS is in convergent orientation with the bait RSS and as inversional if the prey cryptic RSS is in the same orientation with the bait RSS.

3C-HTGTS and data analyses

3C-HTGTS was performed as previously described[3] on G1-arrested RAG2-deficient *v-Abl* cells[3,5–7,26]. Reference genomes were the same as used in HTGTS-V(D)J-seq data analyses described above. To better normalize 3C-HTGTS libraries and reduce the impact of the level of self-ligation (circularization), the high peaks upstream of the bait site were filtered out, following the same rationale as described for 4C-seq[45]. For iEκ-baited 3C-HTGTS libraries, we removed bait site peaks in the chr. 6:70,675,300–70,675,450 region; For *Cer* CBE1-baited 3C-HTGTS libraries, we removed bait site peaks in chr. 6:70,659,550–70,659,700 region; For *Sis* CBE2-baited 3C-HTGTS libraries, we removed bait site peaks in chr. 6:70,664,600–70,664,800 region; For IGCR1 CBE1-baited 3C-HTGTS libraries, we removed bait site peaks in the chr12:114,740,239–114,740,353 region. Then, only the junctions inside of a genomic region (chr. 6:64,515,000–73,877,000 for the entire *Igk* locus; chr. 12:111,453,935–120,640,000 for the entire *Igh* locus; chr. 6:64,515,000–70,658,827 and chr. 12:111,453,935-114,824,843 for the *Igh–Igk* hybrid-Vκ locus) encompassing the entire Ig locus were retained (see details in Code availability). After processing as described above, the retained junctions of the 3C-HTGTS libraries were further normalized to 50,827 total number of junctions, which is the junction number recovered from the smallest library in the set of libraries being compared. The sequences of primers used for generating 3C-HTGTS libraries are listed in Supplementary Table 1.

Unlike ChIP-seq, the junctions of 3C-HTGTS data are discontinuously distributed on the genome, but mainly on the enzyme cutting sites

(CATG by NlaIII). To call peaks for 3C-HTGTS data, we first collapsed the junction signals to nearby enzyme cutting sites, and discarded signals far away (>10 bp) from enzyme cutting sites. Then, we only focused on the cutting sites with signals, calculated the median with a moving window of 101 cutting sites (one centre, 50 left, and 50 right sites). We did a Poisson test for each site, with the median as a conservative over-estimation of the lambda parameter of Poisson distribution. Based on the raw *P* values from the Poisson test, we calculated Bonferroni-adjusted *P* values, called peak summits at the sites with adjusted *P* value < 0.05, and determined the range of peak region by progressively extending the two sides to the sites that have local maximum raw *P* value and also the raw *P* values ≥ 0.05. Nearby overlapping peak regions were merged as one peak region, and only the 'best' (defined by lowest *P* value) summit was kept after merging. Finally, for each group of multiple repeats, we merged the overlapping peak regions from all repeats, and counted the number of supporting repeats for each merged peak region. We defined and only kept the 'robust' peak regions that were supported by >50% of the repeats (that is, ≥ 2 supporting repeats among 2 or 3 repeats, or ≥ 3 supporting repeats among 4 or 5 repeats), and the 'best' (defined by lowest *P* value) summit information was reported.

We further annotated and quantified the features underlying each of the robust 3C-HTGTS peak region ±1 kb. We focused on CBEs, E2A-binding sites, and transcription. For CBEs, we first scanned the possible CBEs by MEME-FIMO using the CTCF motif record (MA0139.1) in JASPAR 2018 core vertebrate database. We applied MACS2 to call peaks in the three repeats of published CTCF ChIP-seq data in parental *v-Abl* line[6], and only kept 'reliable' CBEs with motif score > 13 and overlapping with peaks called in ≥2 repeats. We counted the number of reliable CBEs within each of the robust 3C-HTGTS peak region ±1 kb, and defined them as having an underlying CBE if the number ≥ 1. For E2A-binding sites, we applied MACS2 to get the signal bigwig file from the published E2A ChIP-seq data[46], and then annotated the maximum E2A ChIP-seq signal value within each of the robust 3C-HTGTS peak region ±1 kb. We defined peaks having underlying E2A site if the maximum signal ≥ 0.5. For transcription, we annotated the maximum and the average signal of the three repeats of published GRO-seq data in parental *v-Abl* line[6], and defined a peak as having transcription if the maximum signal ≥40 or the average signal ≥10 in ≥2 repeats. See details in Code availability.

Quantification and statistical analysis

Graphs were generated using GraphPad Prism 10, Origin 2023b and R version 3.6.3. After normalization in each sample, 3C-HTGTS, ChIP-seq and GRO-seq signals of multiple repeats were merged as mean ± s.e.m. of the maximum value in each repeat in each bin, after dividing the plotting region into 1,000 bins (Fig. 2m and Extended Data Fig. 2) or 200 bins (Supplementary Data 1). Unpaired, two-sided Welch's *t*-test was used to compare total rearrangement levels between indicated samples, with *P* values presented in relevant figure legends. Pearson correlation coefficient (*r*) and the corresponding *P* value were calculated to determine the similarity in Vκ usage pattern between indicated samples after calculating the average usage among repeats, and are presented in relevant figure legends.

Availability of materials

All plasmids, cell lines and mouse lines generated in this study are available from the authors upon request.

Reporting summary

Further information on research design is available in the Nature Portfolio Reporting Summary linked to this article.

Data availability

High-throughput sequencing data reported in this study have been deposited in the Gene Expression Omnibus (GEO) database under the accession number GSE263124, with subseries GSE254039 for HTGTS-V(D)J-seq data and GSE263123 for 3C-HTGTS data. The consensus CTCF-binding motif was extracted from JASPAR 2018 core vertebrate database (http://jaspar2018.genereg.net/matrix/MA0139.1). Source data are provided with this paper.

Code availability

HTGTS-V(D)J-seq and 3C-HTGTS data were processed through published pipelines as previously described[43]. Specifically, the pipelines analysing HTGTS data are available at http://robinmeyers.github.io/transloc_pipeline/. Newly developed pipelines for off-targets filtering on cryptic RSS and 3C-HTGTS normalization and peak calling are available at https://github.com/Yyx2626/HTGTS_related.

41. Dai, H.-Q. et al. Direct analysis of brain phenotypes via neural blastocyst complementation. *Nat. Protoc.* **15**, 3154–3181 (2020).
42. Chen, J., Lansford, R., Stewart, V., Young, F. & Alt, F. W. RAG-2-deficient blastocyst complementation: an assay of gene function in lymphocyte development. *Proc. Natl Acad. Sci. USA* **90**, 4528–4532 (1993).
43. Hu, J. et al. Detecting DNA double-stranded breaks in mammalian genomes by linear amplification–mediated high-throughput genome-wide translocation sequencing. *Nat. Protoc.* **11**, 853–871 (2016).
44. Kos, J. T. et al. Characterization of extensive diversity in immunoglobulin light chain variable germline genes across biomedically important mouse strains. Preprint at *bioRxiv* https://doi.org/10.1101/2022.05.01.489089 (2022).
45. Krijger, P. H. L., Geeven, G., Bianchi, V., Hilvering, C. R. E. & de Laat, W. 4C-seq from beginning to end: A detailed protocol for sample preparation and data analysis. *Methods* **170**, 17–32 (2020).
46. Lin, Y. C. et al. A global network of transcription factors, involving E2A, EBF1 and Foxo1, that orchestrates B cell fate. *Nat. Immunol.* **11**, 635–643 (2010).
47. Vettermann, C., Timblin, G. A., Lim, V., Lai, E. C. & Schlissel, M. S. The proximal J kappa germline-transcript promoter facilitates receptor editing through control of ordered recombination. *PLoS ONE* **10**, e0113824 (2015).
48. Alt, F. W. & Baltimore, D. Joining of immunoglobulin heavy chain gene segments: implications from a chromosome with evidence of three D–JH fusions. *Proc. Natl Acad. Sci. USA* **79**, 4118–4122 (1982).
49. Wang, H. et al. Widespread plasticity in CTCF occupancy linked to DNA methylation. *Genome Res.* **22**, 1680–1688 (2012).
50. Jing, D. et al. Lymphocyte-specific chromatin accessibility pre-determines glucocorticoid resistance in acute lymphoblastic leukemia. *Cancer Cell* **34**, 906–921 (2018).

Acknowledgements The authors thank members of the Alt laboratory for contributions to the study, particularly H.-L. Cheng for providing the TC1 ES cell line and advice on ES cell culture, X. Zhang for RAG-expressing retrovirus plasmids, A. M. Chapdelaine-Williams, K. Johnson and L. V. Francisco for help with blastocyst injection and mouse care, and J. Hu for preliminary bioinformatics analyses. This work was supported by NIH Grant R01 AI020047 (to F.W.A.). H.H. and X. Li are supported by a Cancer Research Institute Irvington Postdoctoral Fellowship (CRI5352, CRI4203 to H.H. and CRI5278 to X. Li). Z.B. was supported by a CRI fellowship. F.W.A. is an investigator of the Howard Hughes Medical Institute.

Author contributions F.W.A., H.H. and Y.Z. designed the overall study with help from X. Li. Y.Z., X. Li and H.H. performed most of the experiments. H.H. and J.L. generated Vκ-inversion mice and the Vκ-inversion *v-Abl* lines and performed related experiments with help from K.E.G. H.H. generated the single Jκ5 *v-Abl* cell system and performed related experiments. X. Li generated single Jκ1 *v-Abl* cells and performed related experiments. H.H. and Y.Z. generated the *Igk*-RC and *Igh*-RC inversions and performed related experiments. Y.Z. generated translocation lines and performed related experiments and analysed relative strength of RSSs. Y.Z. and X. Li generated RSS replacements and performed related experiments with help from T.Z. H.H. generated *Cer* and/or *Sis*-deleted and proximal Vκ domain-deleted, single Jκ5 allele cells, and performed related experiments. X. Lin and A.Y.Y. designed and applied bioinformatics pipelines for data analysis and image integration. A.Y.Y. performed statistical analyses for data correlation and developed the 3C-HTGTS peak-calling algorithm. Z.B., H.H. and Y.Z. performed and analysed 3C-HTGTS experiments including defining *Cer*-interacting sequences. Z.B. generated parental *v-Abl* lines, and developed reagents and approaches important for downstream studies. H.H., Y.Z., X. Li, Z.B. and F.W.A. analysed and interpreted data. Y.Z., H.H., X. Li and F.W.A. designed figures. H.H., Y.Z., X. Li and F.W.A. wrote the paper. Other authors helped to refine the paper. The research was performed in the laboratory of F.W.A.

Competing interests The authors declare no competing interests.

Additional information

Supplementary information The online version contains supplementary material available at https://doi.org/10.1038/s41586-024-07477-y.

Correspondence and requests for materials should be addressed to Frederick W. Alt or Hongli Hu.

Peer review information *Nature* thanks David Schatz and the other, anonymous, reviewer(s) for their contribution to the peer review of this work.

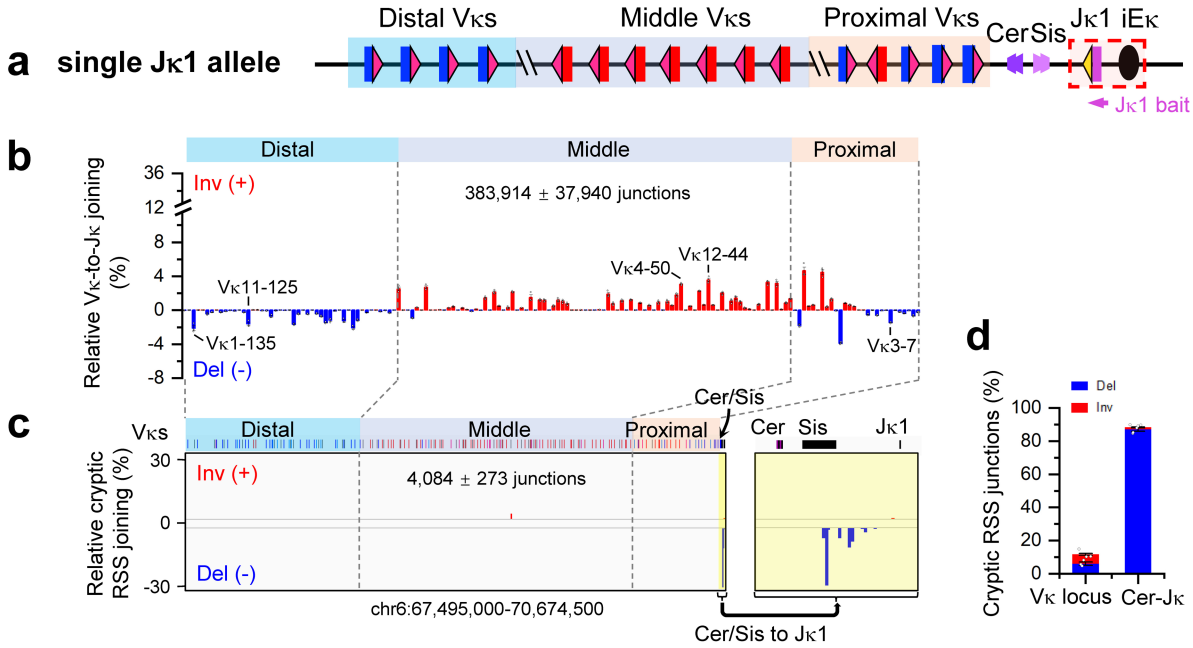

Extended Data Fig. 1 | RAG scanning for primary Vκ-to-Jκ1 rearrangement is terminated within *Sis*. Related to Fig. 2. a, Diagram of single Jκ1 allele *v-Abl* line. **b**, Relative utilization percentage of individual Vκs in single Jκ1 allele line with Jκ1 bait. **c**, Percentage of pooled RAG off-target junctions in *Igκ* locus from single Jκ1 allele line. Right panel: zoom-in to the region between *Cer* and Jκ, highlighted in yellow. **d**, Percentage of inversional (red) and deletional (blue) cryptic RSS junctions within indicated Vκ locus (chr6:67,495,000-70,657,000) and *Cer*-Jκ regions (chr6:70,657,000-70,674,500) from single Jκ1 allele line. Vκ utilization and cryptic RSS data are presented as mean ± s.e.m. from 3 biological repeats. Overall figure presentation is as described in Fig. 2. Note that the total on-target and off-target Jκ1 junctions recovered are, respectively, 5-fold and 8-fold greater than those recovered with a Jκ5 bait, consistent with the greater strength of the Jκ1-RSS[47].

a 3C-HTGTS in RAG-deficient *v-Abl* cells and primary pre-B cells

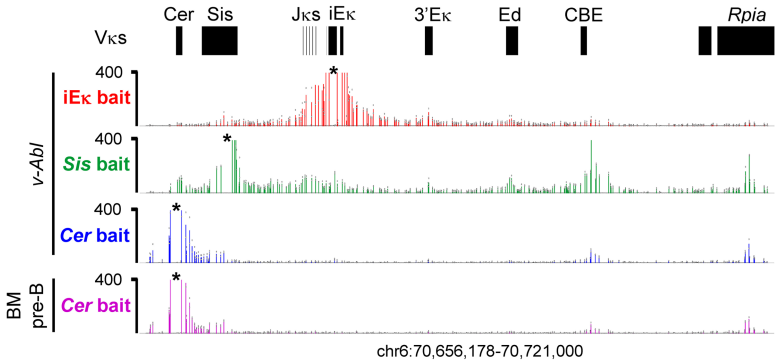

b *Cer*-bait 3C-HTGTS peaks and underlying features in the Vκ locus from RAG-deficient primary pre-B and *v-Abl* cells

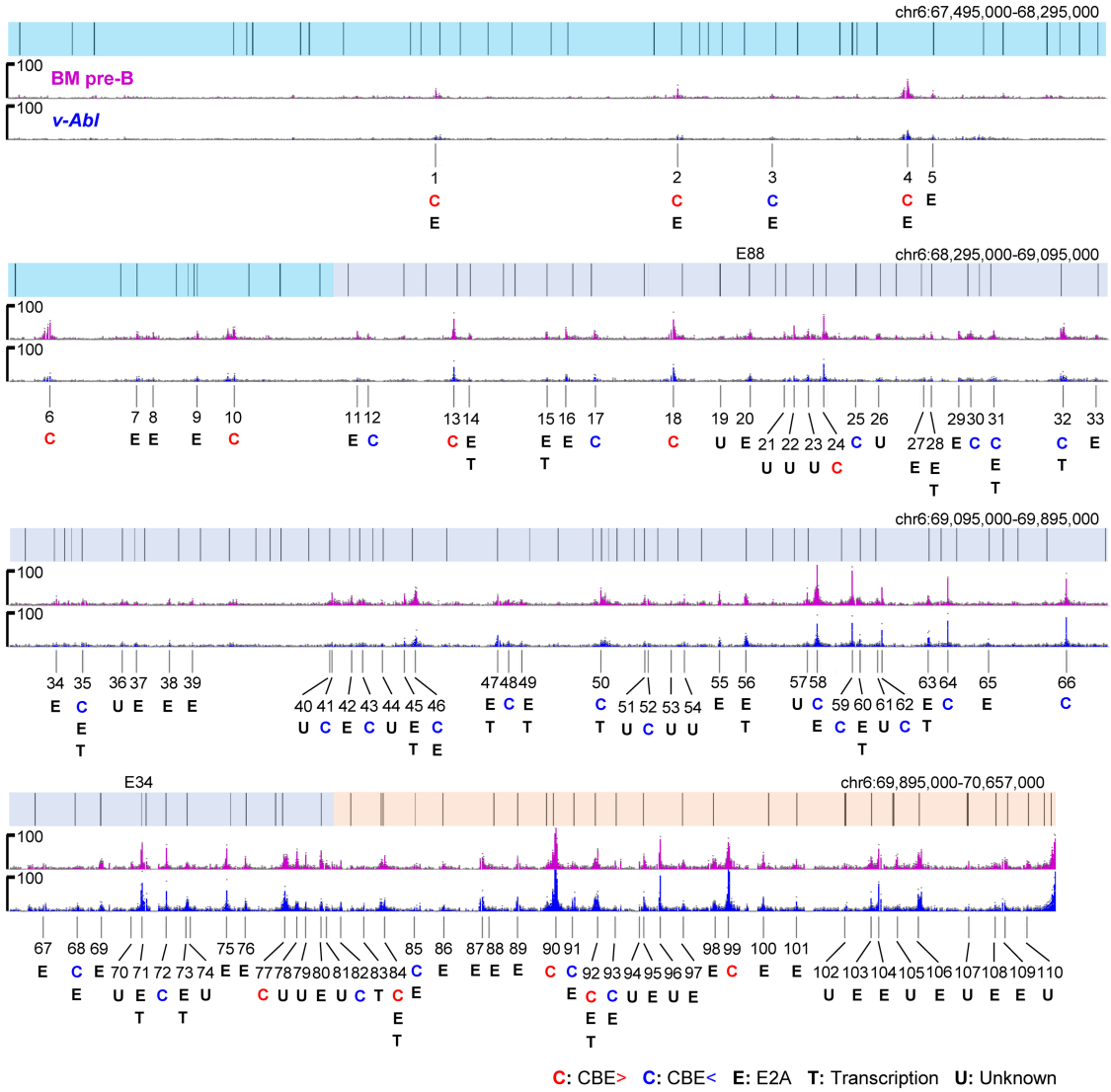

Extended Data Fig. 2 | See next page for caption.

Extended Data Fig. 2 | *Cer* interacts with various loop extrusion impediments across the Vκ locus but not substantially with sequences downstream of *Sis*. Related to Fig. 2. a, 3C-HTGTS profiles in the *Igκ* downstream region from *Cer* to the downstream *Rpia* gene from RAG-deficient *v-Abl* cells, baiting from iEκ (red), *Sis* CBE2 (green) and *Cer* CBE1 (blue) and from RAG-deficient primary pre-B cells baiting from *Cer* CBE1 (pink). Black asterisks indicate the location of baits. **b**, 3C-HTGTS interaction profiles across the Vκ locus when baiting from *Cer* CBE1 in RAG-deficient primary pre-B (pink) and *v-Abl* (blue) cells. *Cer* interaction peaks and their underlying features in the Vκ locus are shown. A total of 110 peaks were called to be significantly above background in either primary pre-B cells or *v-Abl* cells. Peaks are indicated with black lines and numbered according to their locations from distal to proximal. For each peak, underlying features within ± 1 kb are indicated, including rightward CBE ("C" in red), leftward CBE ("C" in blue), E2A-binding sequence ("E") and transcription ("T"). Peaks without any obvious underlying features are labeled as unknown ("U"). CBE annotation and transcription were determined based on published CTCF ChIP-seq and GRO-seq data in RAG-deficient *v-Abl* cells[6]. E2A binding was determined based on published E2A ChIP-seq data in RAG-deficient primary pro-B cells[46]. See Methods for more details. 3C-HTGTS data are presented as mean value from 2 biological repeats.

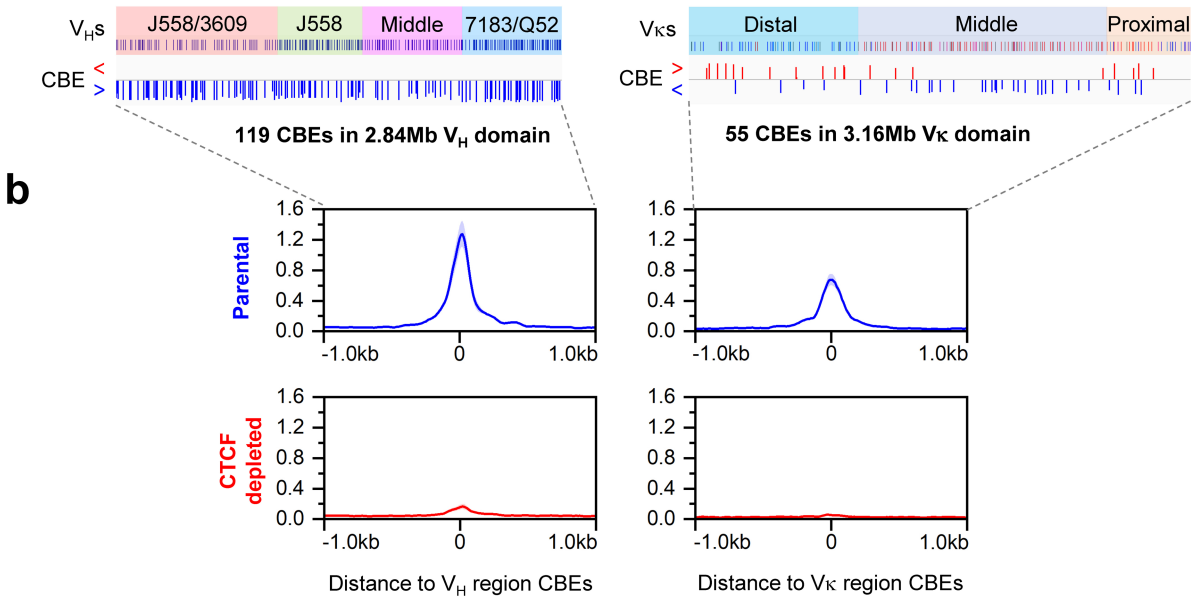

Extended Data Fig. 3 | V_H locus CBEs are more dense and more potent than Vκ locus CBEs. Related to Fig. 2. a, Locations of CBEs in the V_H locus (left) and Vκ locus (right). There are 119 annotated CBEs in the 2.84 Mb V_H locus and 55 annotated CBEs in the 3.16 Mb Vκ locus. The two loci are shown on the same genomic scale to reflect the difference in CBE density. In the Vκ locus, rightward CBEs are shown in red, leftward CBEs are in blue. In the V_H locus, leftward CBEs are shown in red, rightward CBEs are in blue. **b**, Average enrichment of CTCF ChIP-seq signal within ±1 kb region across all annotated CBEs in the V_H locus (left) and Vκ locus (right) in RAG-deficient parental *v-Abl* cells (blue) or CTCF-depleted *v-Abl* cells (red). Data are presented as average signal counts (solid blue or red line) ± s.e.m. (blue or red shade) from 3 biological repeats. The CTCF ChIP-seq data shown were extracted from data deposited in the context of a prior study of RAG-deficient parental and CTCF-depleted *v-Abl* cells[6].

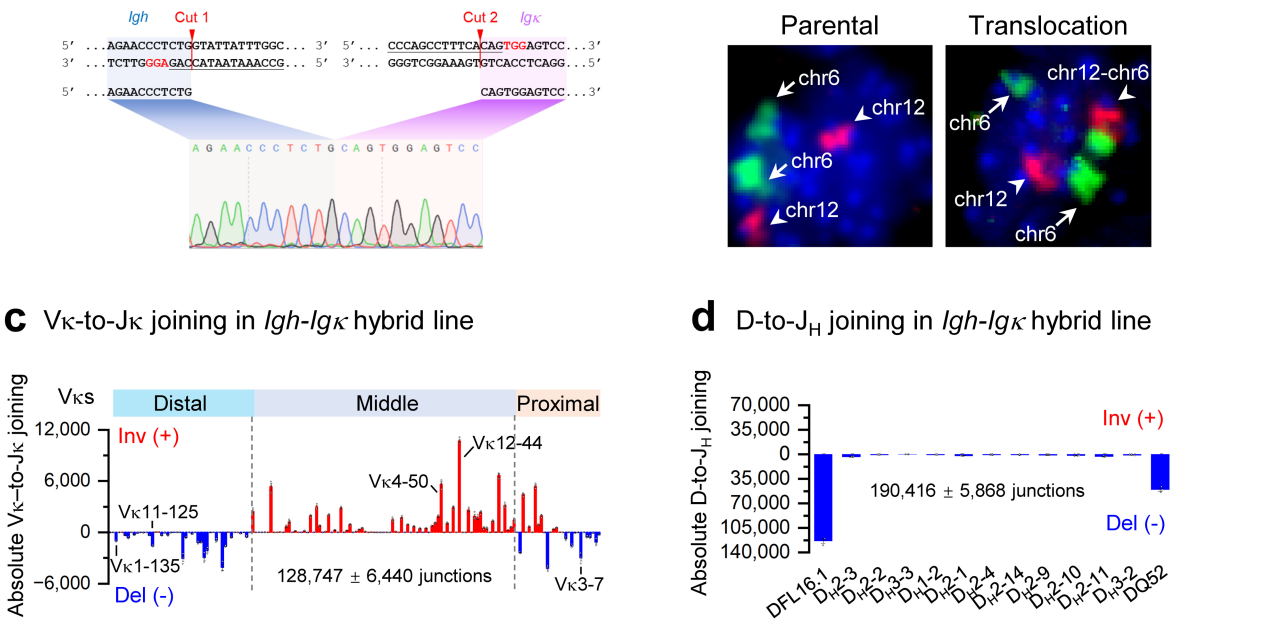

Extended Data Fig. 4 | *Igh-Igκ* hybrid line generated by targeted chromosomal translocation maintains normal D-to-J_H and Vκ-to-Jκ rearrangements. Related to Fig. 4. a, Confirmation of translocation junction in *Igh-Igκ* hybrid *v-Abl* line (shown in Fig. 4a) by PCR/Sanger sequencing. The sgRNA sequences are underlined, sgRNA cut sites are indicated by red arrows, and the Cas9 PAM sequences are labeled in red. **b**, Whole chromosome painting results with probes tiling chromosome 6 (green) and chromosome 12 (red) in single Jκ5-single *Igh v-Abl* cells ("Parental", left) and *Igh-Igκ* hybrid *v-Abl* cells ("Translocation", right). After translocation, a chr12-chr6 fusion chromosome is detected with half of chr6 appended onto chr12. The reciprocal translocation also placed the small telomeric portion (~7 Mb) of chr12 onto chr6, which is below the detectable size of painting experiments. **c**, Absolute level of individual Vκ-to-Jκ joins in *Igh-Igκ* hybrid line with Jκ5 bait. **d**, Absolute level of individual D-to-J_H joining in *Igh-Igκ* hybrid line with J_H1-4 bait. Vκ and D usage data are presented as mean ± s.e.m. from 3 biological repeats.

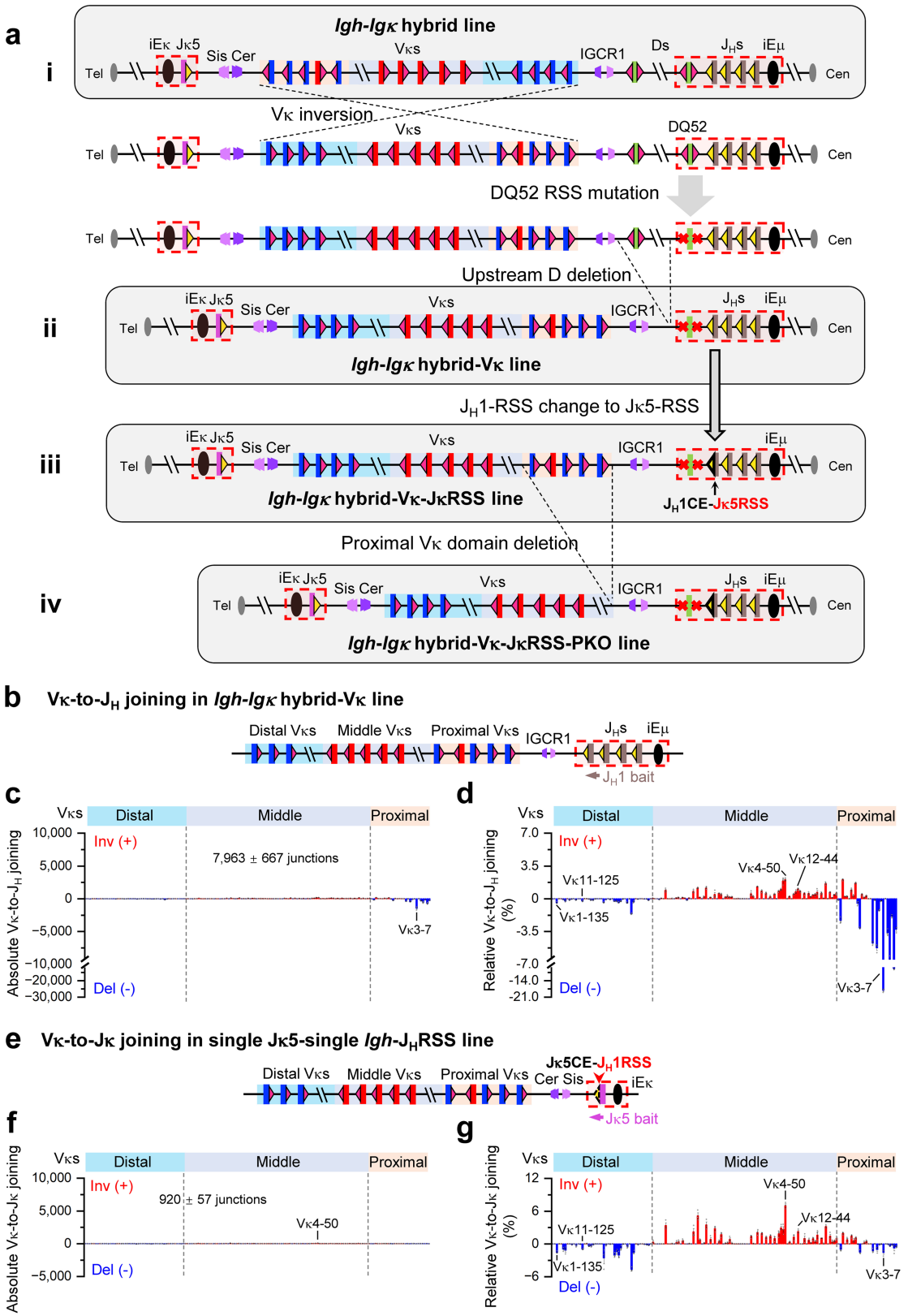

Extended Data Fig. 5 | See next page for caption.

Extended Data Fig. 5 | Genetic modifications in the *Igh-Igκ* hybrid line and single Jκ5 allele line. Related to Fig. 4. a, Diagram of the strategy for various genetic modifications in the *Igh-Igκ* hybrid *v-Abl* line. In brief: (**i**) Diagram of the *Igh-Igκ* hybrid line. (**ii**) Diagram of the *Igh-Igκ* hybrid-Vκ line which was generated from the *Igh-Igκ* hybrid line by inverting the whole Vκ locus, mutating both RSSs of DQ52, and deleting all upstream Ds, as illustrated in the diagrams just above. (**iii**) Diagram of the *Igh-Igκ* hybrid-Vκ-JκRSS line which was generated from the *Igh-Igκ* hybrid-Vκ line by replacing the J_H1-23RSS with a Jκ5-23RSS. (**iv**) Diagram of the *Igh-Igκ* hybrid-Vκ-JκRSS-PKO line which was generated from the *Igh-Igκ* hybrid-Vκ-JκRSS line by deleting the proximal Vκ domain. See Methods for more details. **b**, Diagram of *Igh-Igκ* hybrid-Vκ line, as shown in **a**(**ii**). **c**, Absolute level, and **d**, relative percentage of individual Vκ-to-J_H joins in *Igh-Igκ* hybrid-Vκ line with J_H1 bait. The patterns of distal and middle Vκ usage in the *Igh-Igκ* hybrid-Vκ line (**d**) and the single Jκ5-single *Igh* line (Fig. 4e) are similar (Two-sided Pearson's $r = 0.70$, $P = 2.2e\text{-}21$). **e**, Illustration of single Jκ5-single *Igh*-J_HRSS line, in which Jκ5-23RSS was replaced with J_H1-23RSS. **f**, Absolute level, and **g**, relative percentage of individual Vκ-to-Jκ joins in single Jκ5-single *Igh*-J_HRSS line with Jκ5 bait. Total rearrangement level in **f** is 100-fold lower than that in Fig. 4e ($P = 0.0006$; unpaired, two-sided Welch *t*-test). Vκ usage data are presented as mean ± s.e.m. from 3 biological repeats.

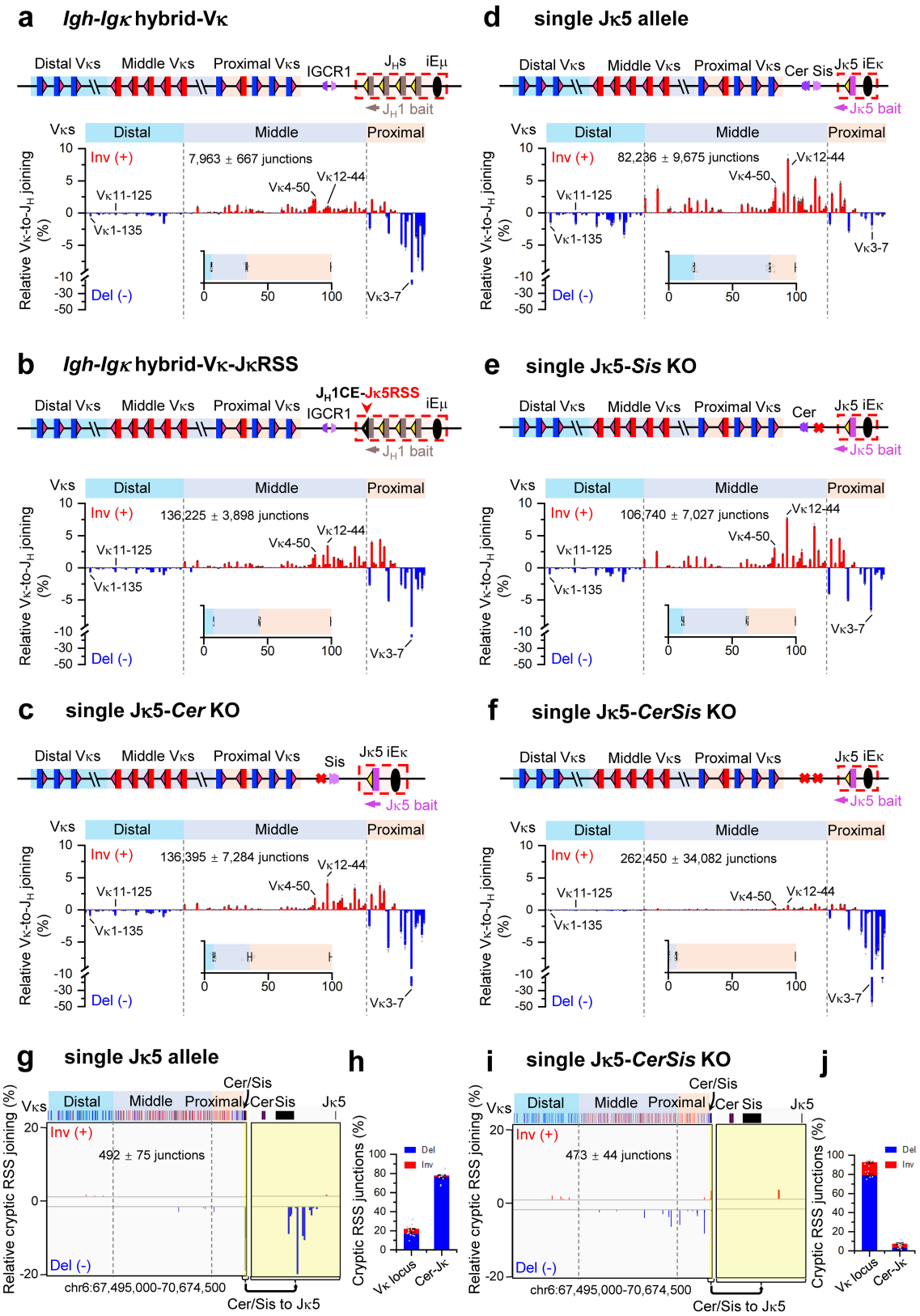

Extended Data Fig. 6 | See next page for caption.

Extended Data Fig. 6 | IGCR1 is a weaker anchor than *Cer-Sis* in preventing over-utilization of proximal deletional Vκs. Related to Fig. 4. a-**f**, Relative utilization percentage of individual Vκs in *Igh-Igκ* hybrid-Vκ line (**a**), *Igh-Igκ* hybrid-Vκ-JκRSS line (**b**), single Jκ5-*Cer* KO line (**c**), single Jκ5 allele line (**d**), single Jκ5-*Sis* KO line (**e**), single Jκ5-*CerSis* KO line (**f**) analyzed with indicated baits. Bar graph in the inset of each panel shows the percentage of distal (blue), middle (gray) and proximal (orange) Vκ domain usage from the corresponding line. **g**, Percentage of pooled RAG off-target junctions in *Igκ* locus from single Jκ5 allele line. Right panel: zoom-in to the region between *Cer* and Jκ, highlighted in yellow. **h**, Percentage of inversional (red) and deletional (blue) cryptic RSS junctions from single Jκ5 allele line within indicated regions as in Fig. 2d. **i**-**j**, RAG off-target profiles in single Jκ5-*CerSis* KO line presented as in **g**-**h**. A group of aberrant pseudo-normal coding-end junctions[48] to sequences near the *Igκ* downstream CBE were excluded[4]. The patterns of Vκ usage in **a**, **b** and **c** are highly similar (**a** and **c**, Two-sided Pearson's $r = 0.91$, $P = 1.5e\text{-}63$; **b** and **c**, Two-sided Pearson's $r = 0.97$, $P = 1.0e\text{-}99$). The data shown in **a** and **d** are the same as that shown in Extended Data Fig. 5d and Fig. 2f, the data shown in **g** and **h** are the same as that shown in Fig. 2g and h, respectively, plotted here for better alignment and comparison with other results. Vκ utilization and cryptic RSS data are presented as mean ± s.e.m. from 3 (**a**,**b**,**e**), 4 (**c**), 7 (**d**,**h**) or 6 (**f**,**j**) biological repeats.

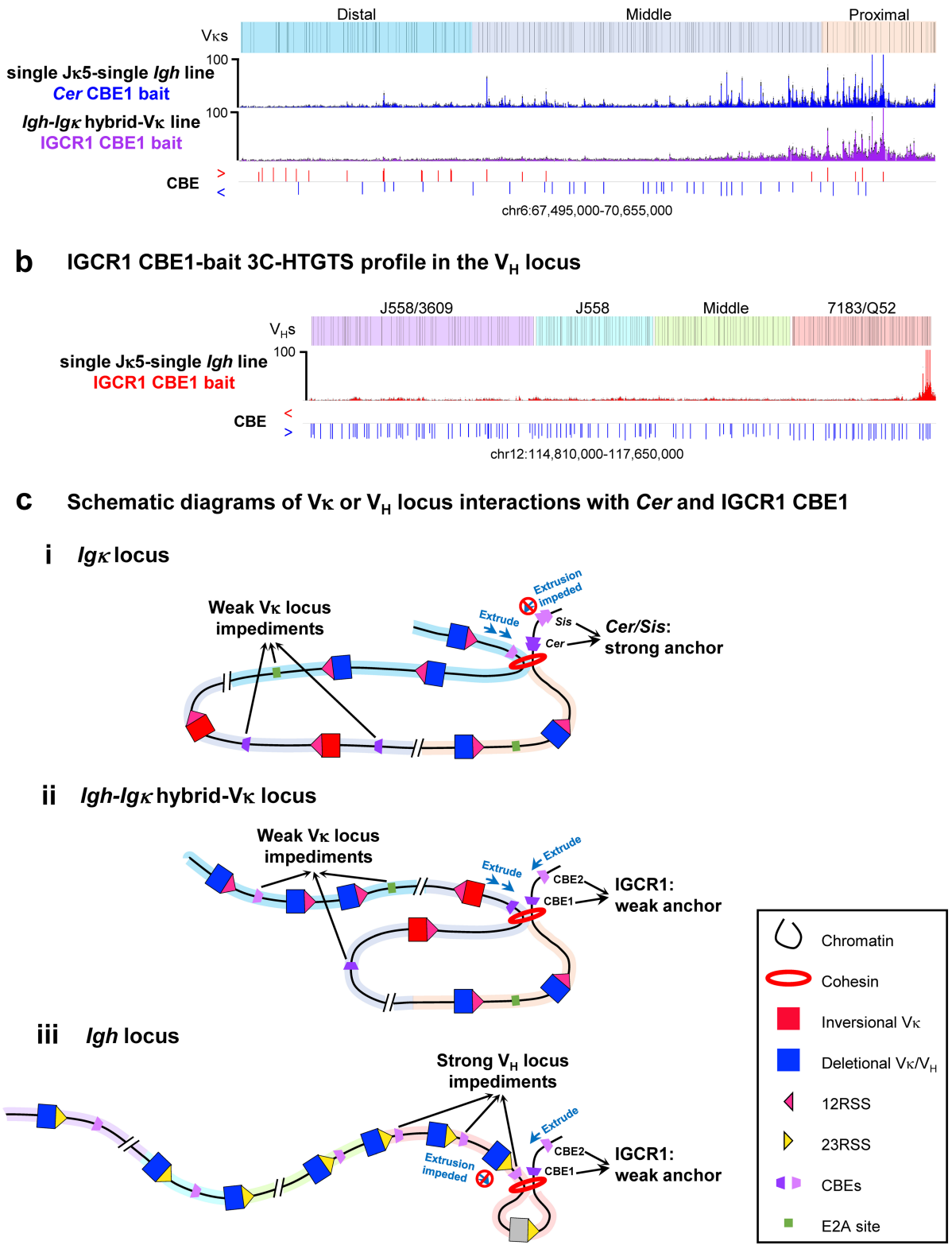

Extended Data Fig. 7 | See next page for caption.

Extended Data Fig. 7 | Interactions of IGCR1 or *Cer-Sis* with V_H or Vκ locus in *v-Abl* cells. Related to Fig. 4 and Extended Data Fig. 3. a, **Upper panel**: 3C-HTGTS profiles in the Vκ locus from single Jκ5-single *Igh v-Abl* line baiting from *Cer* CBE1. **Lower panel**: 3C-HTGTS profiles in the Vκ locus from *Igh-Igκ* hybrid-Vκ *v-Abl* line baiting from IGCR1 CBE1. **b**, 3C-HTGTS profiles in the V_H locus from single Jκ5-single *Igh* line baiting from IGCR1 CBE1. CBE sites are shown in **a** and **b** with orientations labeled as in Extended Data Fig. 3a. 3C-HTGTS data are presented as mean ± s.e.m. from 3 biological repeats (**a**) or as mean value from 2 biological repeats (**b**). **c**, Schematic loop domain illustrations of *Igκ*, *Igh*, and *Igh-Igκ* hybrid-Vκ loci based on 3C-HTGTS data shown in **a** and **b**. (**i**) In *Igκ* locus, the strong anchoring activity of *Cer-Sis*, coupled with relatively weak impediments in the Vκ locus, allows loop extrusion anchored at *Cer* to extend across the distal, middle and proximal Vκ domains, as shown in **a**, **upper panel**. (**ii**) In *Igh-Igκ* hybrid-Vκ locus, loop extrusion anchored at IGCR1 can extend a considerable distance into proximal and middle Vκ domains with weak Vκ locus impediments, but does not extend as far as that in (**i**), because IGCR1 is a less stable anchor than *Cer-Sis* and more likely to be disassembled before loop extrusion has a chance to proceed into the distal Vκ locus, as shown in **a**, **lower panel**. (**iii**) In *Igh* locus without WAPL down-regulation, strong V_H locus impediments only allow loop extrusion to bring the most proximal V_H region to IGCR1, while upstream interactions are completely blocked by the "wall" of proximal V_H CBEs, as shown in **b**. Elements and proteins illustrated are indicated in the box.

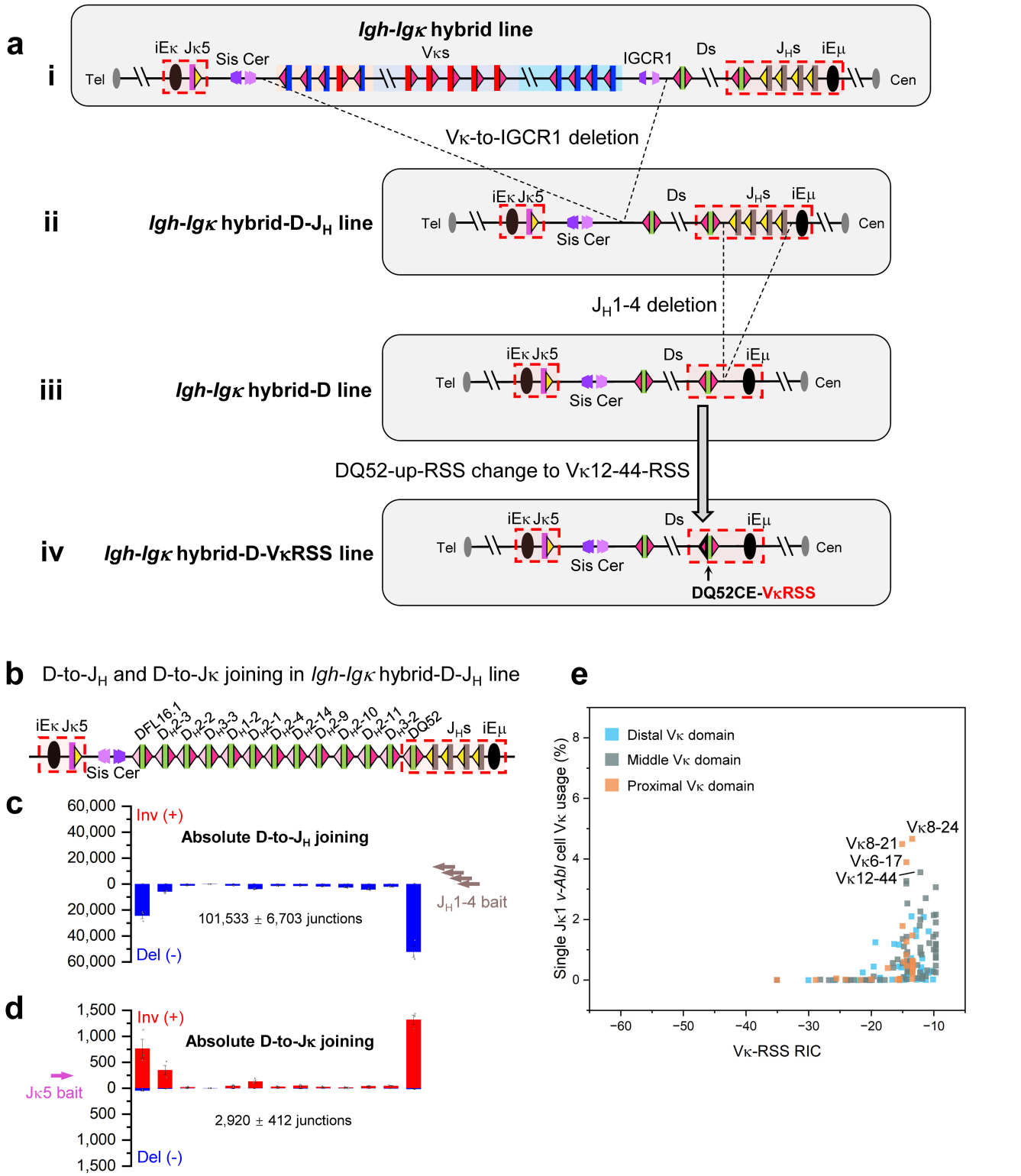

Extended Data Fig. 8 | Genetic modifications in the *Igh-Igκ* hybrid-D line, and correlation of Vκ usage with RIC score. Related to Fig. 5. a, Diagram of the strategy for various genetic modifications in the *Igh-Igκ* hybrid-D *v-Abl* line. (**i**) Diagram of the *Igh-Igκ* hybrid line. (**ii**) Diagram of the *Igh-Igκ* hybrid-D-J_H line which was generated from the *Igh-Igκ* hybrid line by deleting all Vκs and IGCR1. (**iii**) Diagram of the *Igh-Igκ* hybrid-D line which was generated from the *Igh-Igκ* hybrid-D-J_H line by deleting J_H1-4. (**iv**) Diagram of the *Igh-Igκ* hybrid-D-VκRSS line which was generated from the *Igh-Igκ* hybrid-D line by replacing the DQ52 upstream 12RSS with a Vκ12-44 12RSS. See Methods for details. **b**, Diagram of the *Igh-Igκ* hybrid-D-J_H line as illustrated in **a**(**ii**). **c**, Absolute level of D-to-J_H joins baiting from J_H1-4 in the *Igh-Igκ* hybrid-D-J_H line. **d**, Absolute level of D-to-Jκ joins baiting from Jκ5 in the *Igh-Igκ* hybrid-D-J_H line. D utilization data are presented as mean ± s.e.m. from 3 biological repeats. **e**, Comparison of relative Vκ usage in single Jκ1 allele *v-Abl* cells with Vκ-RSS RIC scores. Vκs are color-coded according to the three Vκ domains with names indicated for highly used Vκs.

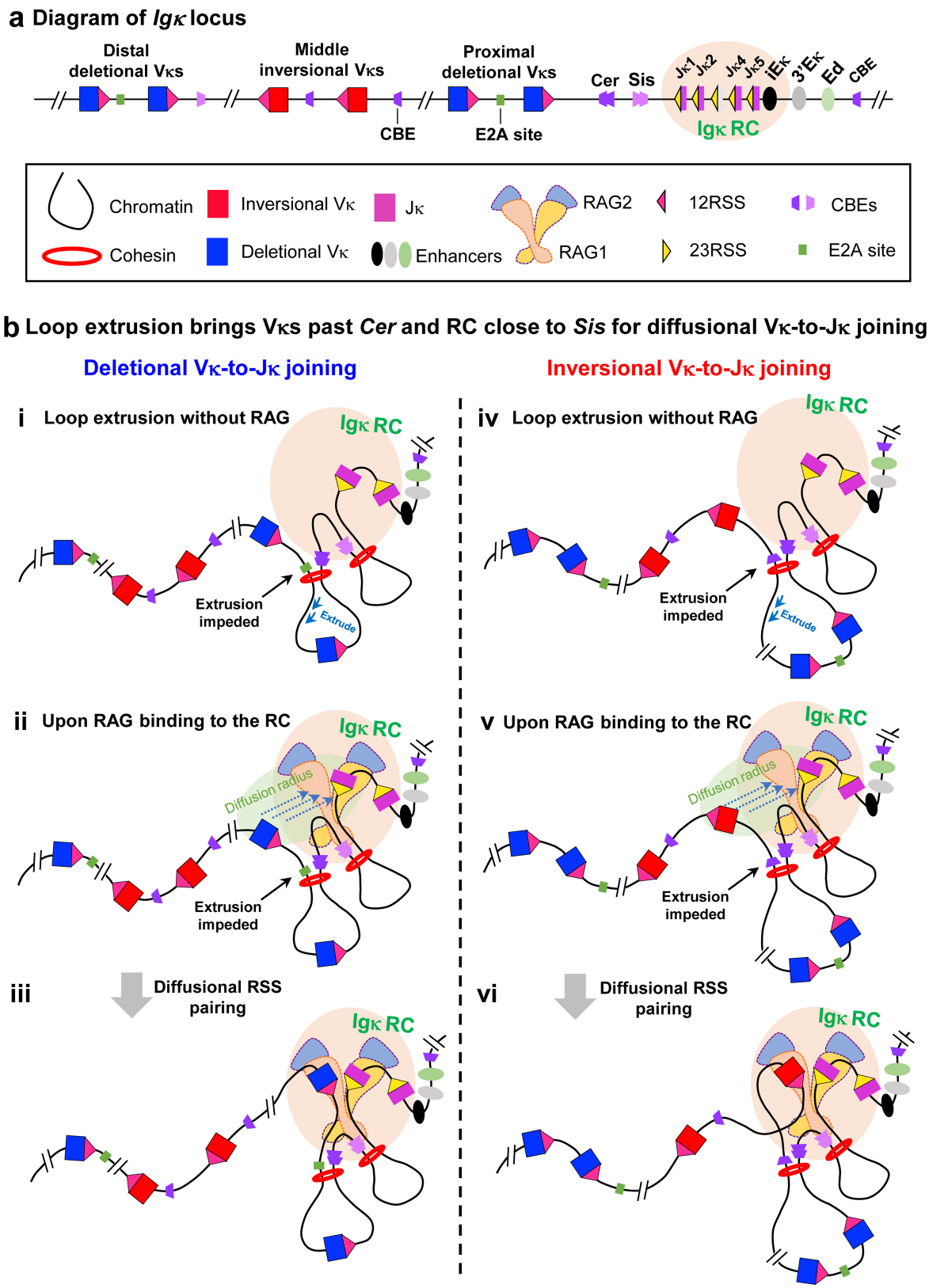

Extended Data Fig. 9 | See next page for caption.

Extended Data Fig. 9 | Working model for short-range diffusion-mediated primary *Igκ* V(D)J recombination. a, Diagram of *Igκ* (not to scale). Elements and proteins illustrated are indicated in the box. **b**, Working model. (**i**) Loop extrusion of downstream chromatin through a cohesin ring impeded in the upstream direction at *Sis* juxtaposes the RC, a downstream impediment, to *Sis*. Simultaneously, loop extrusion of upstream chromatin through a cohesin ring impeded in the downstream direction at *Cer* brings the Vκ locus past *Cer*. (**ii**) During extrusion past *Cer*, relatively weak extrusion impediments, including CBEs and E2A sites (illustrated) across the Vκ locus dynamically impede extrusion at *Cer*, providing more opportunity for Vκ-RSSs to remain in short-range diffusion distance for interactions with RC-bound RAG. (**iii**) Binding of paired strong Vκ-RSSs to the RAG-1 active site across from strong Jκ-RSSs promote robust cleavage and/or joining. (**iv**-**vi**) Only a fraction of Vκ-RSSs brought into diffusion range pair with Jκ-RSSs, allowing extrusion to continue upstream where impediments slow down extrusion past *Cer*, providing opportunity for additional Vκ-RSSs to interact with RC-bound RAG. These panels diagram use of inversional-oriented Vκs, which can interact by the same short-range diffusion process outlined for deletional Vκs. The diagram is simplified to provide a general overview of the proposed mechanism, for which details await high resolution studies. Due to relatively weak *Igκ* impediments, this model is compatible with cohesin loading across the Vκ locus[2]. Also, RAG is likely not continuously bound to the RC[2,7], allowing extrusion to continue past *Cer*. These latter features could allow active RAG-bound RCs to initiate the process at different points across the Vκ locus to optimize diverse Vκ utiliation[2,7]. Human *Igκ*, which undergoes deletional and inversional joining, has *Cer*-*Sis*-like elements in the Vκ-Jκ interval[12,49,50] and high Vκ-RSS RIC scores[33], consistent with employing a similar primary rearrangement mechanism to mouse *Igκ*.

nature portfolio

Corresponding author(s): Frederick W. Alt and Hongli Hu

Last updated by author(s): Apr 11, 2024

Reporting Summary

Nature Portfolio wishes to improve the reproducibility of the work that we publish. This form provides structure for consistency and transparency in reporting. For further information on Nature Portfolio policies, see our Editorial Policies and the Editorial Policy Checklist.

Statistics

For all statistical analyses, confirm that the following items are present in the figure legend, table legend, main text, or Methods section.

n/a	Confirmed
☐	☒ The exact sample size (*n*) for each experimental group/condition, given as a discrete number and unit of measurement
☐	☒ A statement on whether measurements were taken from distinct samples or whether the same sample was measured repeatedly
☐	☒ The statistical test(s) used AND whether they are one- or two-sided *Only common tests should be described solely by name; describe more complex techniques in the Methods section.*
☒	☐ A description of all covariates tested
☐	☒ A description of any assumptions or corrections, such as tests of normality and adjustment for multiple comparisons
☐	☒ A full description of the statistical parameters including central tendency (e.g. means) or other basic estimates (e.g. regression coefficient) AND variation (e.g. standard deviation) or associated estimates of uncertainty (e.g. confidence intervals)
☐	☒ For null hypothesis testing, the test statistic (e.g. *F*, *t*, *r*) with confidence intervals, effect sizes, degrees of freedom and *P* value noted *Give P values as exact values whenever suitable.*
☒	☐ For Bayesian analysis, information on the choice of priors and Markov chain Monte Carlo settings
☒	☐ For hierarchical and complex designs, identification of the appropriate level for tests and full reporting of outcomes
☐	☒ Estimates of effect sizes (e.g. Cohen's *d*, Pearson's *r*), indicating how they were calculated

Our web collection on statistics for biologists contains articles on many of the points above.

Software and code

Policy information about availability of computer code

Data collection	Next generation sequencing data were collected via Illumina sequencing platforms (NextSeq 550 and NextSeq 2000). NextSeq 550 control software (2.2.0) and NextSeq 1000/2000 control software (1.5.0.42699) were used for high-throughput sequencing data collection. Data generated from NextSeq 550 or NextSeq 2000 were demultiplexed via TranslocPreprocess.pl, a published pipeline available at http://robinmeyers.github.io/transloc_pipeline/.
Data analysis	HTGTS-V(D)J-seq and 3C-HTGTS data were processed via the published pipeline (http://robinmeyers.github.io/transloc_pipeline/). Newly developed pipelines for off-targets filtering on cryptic RSS and 3C-HTGTS normalization and peak calling are available at https://github.com/Yyx2626/HTGTS_related. GraphPad Prism 10, Origin 2023b and R 3.6.3 were used for statistical analysis and graph visualization. IGV (2.11.1) was used to visualize RAG off-target data. ImageJ (1.53q) was used for fluorescence image processing.

For manuscripts utilizing custom algorithms or software that are central to the research but not yet described in published literature, software must be made available to editors and reviewers. We strongly encourage code deposition in a community repository (e.g. GitHub). See the Nature Portfolio guidelines for submitting code & software for further information.

Data

Policy information about availability of data

All manuscripts must include a data availability statement. This statement should provide the following information, where applicable:

- Accession codes, unique identifiers, or web links for publicly available datasets
- A description of any restrictions on data availability
- For clinical datasets or third party data, please ensure that the statement adheres to our policy

HTGTS-V(D)J-Seq and 3C-HTGTS sequencing data reported in this study have been deposited in the GEO database under the accession number GSE263124, with GSE254039 for HTGTS-V(D)J-Seq data and GSE263123 for 3C-HTGTS data. The consensus CTCF binding motif was extracted from JASPAR 2018 core vertebrate database (http://jaspar2018.genereg.net/matrix/MA0139.1).

Research involving human participants, their data, or biological material

Policy information about studies with human participants or human data. See also policy information about sex, gender (identity/presentation), and sexual orientation and race, ethnicity and racism.

Reporting on sex and gender	N/A
Reporting on race, ethnicity, or other socially relevant groupings	N/A
Population characteristics	N/A
Recruitment	N/A
Ethics oversight	N/A

Note that full information on the approval of the study protocol must also be provided in the manuscript.

Field-specific reporting

Please select the one below that is the best fit for your research. If you are not sure, read the appropriate sections before making your selection.

☒ Life sciences ☐ Behavioural & social sciences ☐ Ecological, evolutionary & environmental sciences

For a reference copy of the document with all sections, see nature.com/documents/nr-reporting-summary-flat.pdf

Life sciences study design

All studies must disclose on these points even when the disclosure is negative.

Sample size	No statistical methods were used to predetermine sample size for all experiments. Sample sizes were chosen based on previous studies in this field (Dai et al., Nature 2021; Ba et al., Nature 2020) that used similar sample sizes to generate reproducible results.
Data exclusions	No data was excluded from analysis.
Replication	All samples were analyzed with both biological and experimental repeats as detailed in the relevant text and figure legends. All attempts for replication were successful.
Randomization	Experiments were not randomized. Each experiment was performed with identified control and mutant strains. Randomization was not relevant to the study as the study does not involve participant groups.
Blinding	Investigators were not blinded to allocation during experiments and outcome assessment. Blinding was not possible as investigators need to verify the control and matched mutant strains before each experiment. Also, based on previous studies in this field, these assays do not require blinding.

Reporting for specific materials, systems and methods

We require information from authors about some types of materials, experimental systems and methods used in many studies. Here, indicate whether each material, system or method listed is relevant to your study. If you are not sure if a list item applies to your research, read the appropriate section before selecting a response.

Materials & experimental systems

n/a	Involved in the study
☐	☒ Antibodies
☐	☒ Eukaryotic cell lines
☒	☐ Palaeontology and archaeology
☐	☒ Animals and other organisms
☒	☐ Clinical data
☒	☐ Dual use research of concern
☒	☐ Plants

Methods

n/a	Involved in the study
☒	☐ ChIP-seq
☒	☐ Flow cytometry
☒	☐ MRI-based neuroimaging

Antibodies

Antibodies used

anti-B220-APC (eBioscience, #17-0452-83), 1:1000
anti-CD43-PE (BD Biosciences, #553271), 1:400
anti-IgM-FITC (eBioscience, #11-5790-81), 1:500

Validation

anti-B220-APC (eBioscience, #17-0452-83), anti-CD43-PE (BD Biosciences, #553271) and anti-IgM-FITC (eBioscience, #11-5790-81) have been confirmed by FACS in published papers including (except this study): Dai, H.-Q. et al. Loop extrusion mediates physiological Igh locus contraction for RAG scanning. Nature 590, 338–343 (2021).

Eukaryotic cell lines

Policy information about cell lines and Sex and Gender in Research

Cell line source(s)

The primary pre-B cells were derived from bone marrows of 4-6-week-old WT, Vk inverted and Igh pre-rearranged; Rag2-/- 129SV mice in both genders (male mice and female mice are equally used in the experiments). The Wapl-degron immortalized v-Abl cell lines and derivatives were generated by retroviral infection of primary pro-B cells derived from initial RAG1-deficient; Em-Bcl2 transgenic female C57BL/6 mice with pMSCV-v-Abl retrovirus, made in our lab. All other immortalized v-Abl cell lines and derivatives were generated by retroviral infection of primary pro-B cells derived from initial RAG2-deficient; Em-Bcl2 transgenic male 129SV mice with pMSCV-v-Abl retrovirus, made in our lab. See Methods for details.

Authentication

All cell lines were authenticated by PCR genotyping and Sanger sequencing. v-Abl cell line with targeted chromosomal translocation was also authenticated by whole chromosome painting. See Methods for details. Sequences of all sgRNAs and oligos used are listed in Supplementary Table 1.

Mycoplasma contamination

All ES cell lines used for targeting and RAG-deficient blastocyst complementation injections were confirmed to be mycoplasma free. v-Abl cell lines were not tested for mycoplasma contamination.

Commonly misidentified lines
(See ICLAC register)

None

Animals and other research organisms

Policy information about studies involving animals; ARRIVE guidelines recommended for reporting animal research, and Sex and Gender in Research

Laboratory animals

All mouse work was performed in compliance with all the relevant ethical regulations established by the Institutional Animal Care and Use Committee (IACUC) of Boston Children's Hospital and under protocols approved by the IACUC of Boston Children's Hospital. Mice were maintained on a 14-h light/10-h dark schedule in a temperature (22±3°C)/humidity (35%~70%±5%)-controlled environment, with food and water provided ad libitum. We used 4-6-week-old WT, Vk inverted and Igh pre-rearranged; Rag2-/- 129SV mice, including both males and females, for isolating primary pre-B cells from bone marrow. For each HTGTS-V(D)J-seq experiment, we sacrificed 7 mice for both WT mice and Vk inverted mice. For each 3C-HTGTS experiment, we pooled cells from 3-4 mice per sample and prepared 2 samples per experimental condition.

Wild animals

The study did not involve wild animals.

Reporting on sex

Both male and female mice from WT, Vk inverted and Igh pre-rearranged; Rag2-/- 129SV colonies were used in experiments.

Field-collected samples

The study did not involve samples collected from the field.

Ethics oversight

All mouse work were performed in compliance with all the relevant ethical regulations established by the Institutional Animal Care and Use Committee (IACUC) of Boston Children's Hospital and under protocols approved by the IACUC of Boston Children's Hospital.

Note that full information on the approval of the study protocol must also be provided in the manuscript.

Plants

Seed stocks	N/A
Novel plant genotypes	N/A
Authentication	N/A